SIAM J. APPL. MATH.
Vol. 66, No. 5, pp. 1793–1824

CYLINDER BUCKLING: THE MOUNTAIN PASS AS AN ORGANIZING CENTER*

JIŘÍ HORÁK†, GABRIEL J. LORD‡, AND MARK A. PELETIER§

Abstract. We revisit the classical problem of the buckling of a long thin axially compressed cylindrical shell. By examining the energy landscape of the perfect cylinder, we deduce an estimate of the sensitivity of the shell to imperfections. Key to obtaining this estimate is the existence of a mountain pass point for the system. We prove the existence on bounded domains of such solutions for almost all loads and then numerically compute example mountain pass solutions. Numerically the mountain pass solution with lowest energy has the form of a single dimple. We interpret these results and validate the lower bound against some experimental results available in the literature.

Key words. imperfection sensitivity, subcritical bifurcation, single dimple

AMS subject classifications. 35J50, 35J35, 35J60, 35G30, 35Q72

DOI. 10.1137/050635778

1. Introduction.

1.1. Buckling of cylinders under axial loading.

A classical problem in structural engineering is the prediction of the load-carrying capacity of an axially loaded cylinder. In addition to being a commonly used structural element, the axially loaded cylinder is the archetype of unstable, imperfection-sensitive buckling, and this has led to a large body of theoretical and experimental research.

In the decades before and after the Second World War, a central problem was understanding the large discrepancy between theoretical predictions and experimental observations, as shown in Figure 1.1. A variety of different explanations has been put forward, but with the experimental work of Tennyson [30] and the theoretical work of Almroth [1] it became clear that this discrepancy is mostly due to imperfections in loading conditions and in the shape of the specimens. Further experimental and theoretical work by many others has confirmed this conclusion [14, 33, 36].

For near-perfect cylinders, the linear and weakly nonlinear theories (see section 1.2) adequately describe the experimental buckling load[1] and the deformation just before failure (see, e.g., [4]). Cylinders used in practical applications, however, are far too imperfect, and thus the weakly nonlinear theory does not apply. From a practical point of view, the problem of predicting the failure load is still open.

There is good reason to believe that it will never be possible to accurately predict failure loads for cylinders that are used in practice. For simple materials, such as metals, it is believed that current numerical methods can describe the local material behavior with enough accuracy that correct prediction of the complete behavior of the cylinder—including its failure—is feasible. This could be achieved provided the geometrical and material imperfections, as well as the loading conditions, are determined

*Received by the editors July 12, 2005; accepted for publication (in revised form) April 6, 2006; published electronically August 22, 2006.
http://www.siam.org/journals/siap/66-5/63577.html
†Universität Köln, Köln, Germany (j.horak@math.uni-koeln.de).
‡Heriot-Watt University, Edinburgh, UK (g.j.lord@ma.hw.ac.uk).
§Technische Universiteit Eindhoven, Eindhoven, The Netherlands (m.a.peletier@tue.nl).
[1]In this paper the terms "experimental buckling load" and "failure load" are used interchangeably.

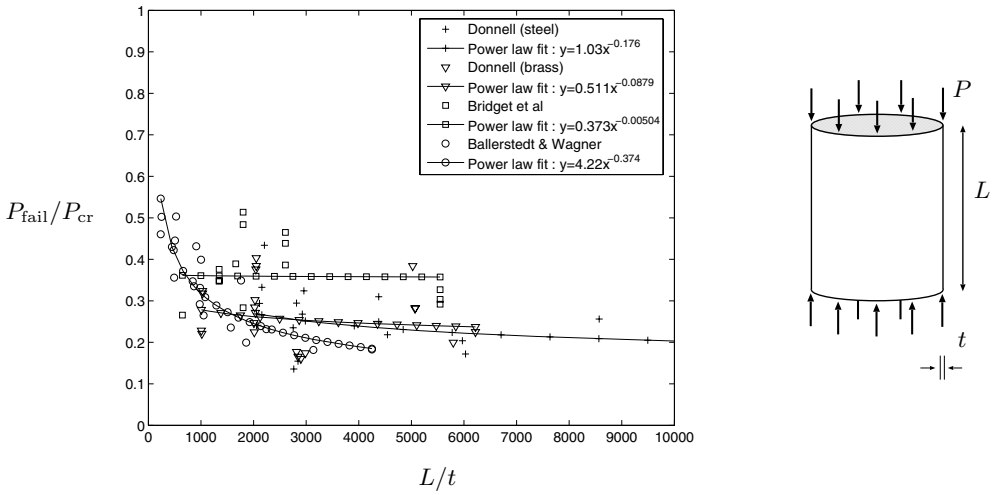

FIG. 1.1. *Experimental data from various research groups, all representing failure loads of axially loaded cylinders. The horizontal axis is the ratio of the cylinder length and the wall thickness; the vertical axis is the ratio of the failure load and the theoretical critical load as predicted for perfect cylinders. Note that all tested cylinders fail at loads significantly lower than that predicted by theory; the latter would correspond to failure load* $P_{\rm fail}/P_{\rm cr} = 1$*, and in some cases failure occurred at less than one-fifth of this value. Power-law fitting lines are added to emphasize the dependence of the failure load on the geometry. The data are from* [10, 7, 5].

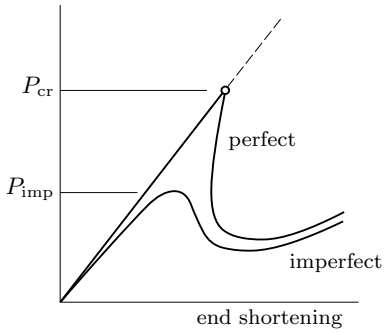

FIG. 1.2. *Illustration of perfect and imperfect bifurcation curves. For the unperturbed system, the undeformed state (the straight line) is always an equilibrium; this state loses stability at a bifurcation point at load* $P_{\rm cr}$*, and a curve of nonzero equilibria branches off. Perturbing the system generically converts the sharp bifurcation into a smooth transition. In the case of the cylinder, the postbuckling path is strongly unstable, and the perturbed path therefore has a lower limit load of* $P_{\rm imp}$.

in sufficient detail. The difficulty lies in the qualifier "in sufficient detail," since an extremely accurate measurement of the geometric imperfections would be necessary [4], and in the design phase both the loading conditions and the geometric and material imperfections in the finalized product are known only in vague terms. Therefore, in recent decades the attention of theoretical research has turned to characterizing the failure load in weaker ways, preferably in the form of a lower (safe) bound.

1.2. Characterizing sensitivity to imperfections. Viewed as a bifurcation problem, the buckling of the cylinder is a subcritical symmetry-breaking pitchfork bifurcation (Figure 1.2). Generically, imperfections in the structure eliminate the

bifurcation and round off the branch of solutions,[2] resulting in a turning point at a load P_{imp} strictly below the critical (bifurcation) load P_{cr} of the perfect structure. In an experiment in which the load is slowly increased, the system will fail (i.e., make a large jump in state space) at load P_{imp}.

Again, if the imperfections in geometry and loading are fully known, then calculation of P_{imp} is a practical rather than a theoretical problem, and we do not address this problem here. For the more difficult question of characterizing P_{imp} under incomplete information, various strategies have been proposed. A classical line of thought originates with Koiter [22], in which the imperfections are chosen a priori within certain finite-dimensional sets. Common choices are the sets spanned by the eigenvector at the bifurcation point of the perfect structure or by the eigenvectors associated with the first n bifurcations. This approach might be termed weakly nonlinear, as it is based on an expansion of the energy close to the bifurcation point, in the directions suggested by the bifurcation point itself. It gives predictions that are correct if the imperfections are very small—much smaller than those encountered in practice.

Since the a priori choice of imperfections is a weak point of this method, a natural step is to optimize over all possible perturbations. Deml and Wunderlich pioneered this approach, in which a numerical algorithm is used to find a "worst geometric imperfection" [9]. This "worst imperfection" is defined as that imperfection that produces a turning point of minimal load. Some constraint on the magnitude of allowable perturbations is necessary, of course, to prevent the running of a steam roller over the cylinder being interpreted as an admissible imperfection. The authors of [9] and [35] first suggest constraining the L^∞-norm of the perturbation displacement, but they immediately replace the L^∞-norm with an L^p-norm for computational convenience.

This method has an interesting aspect that is often glossed over in the engineering literature. By definition, the failure load obtained by this method is a lower bound for the failure load of all systems that have perturbations of lesser or equal magnitude. The measure of magnitude is defined by the choice of constraint. Therefore the choice of constraint on the imperfections is critical, since it implicitly defines a class of imperfections that produce either the same failure load or a higher one.

1.3. Main results. In this paper we follow a related, but distinct, line of reasoning. Instead of studying the actual behavior of imperfect cylinders, we deduce an estimate of the sensitivity to imperfections from the energy landscape of the perfect cylinder. The final result is a lower bound on the failure load similar to the above lower bound, and the approach gives additional insight into the problem.

The key result is the existence of a *mountain pass point*, an equilibrium state that is straddled between two valleys in the energy landscape; one valley surrounds the unbuckled state, and the other contains many buckled, large-deformation states.

This mountain pass point has a number of interesting properties, as follows:

1. It has the appearance of a *single-dimple solution*, a small buckle in the form of a single dent (see Figure 1.3(a)). Single-dimple deformations have appeared in engineering literature in a number of different ways (see section 6), but a theoretical understanding of this phenomenon is still lacking. Localization (concentration) of deformation is commonly known to appear in extended structures [21], and in the cylinder localization in the axial direction has been studied theoretically and numerically [20, 24, 25]. Whether localization

[2] Koiter actually used this elimination of a bifurcation point as a *definition* of "perfect system" and "perturbed system" [22].

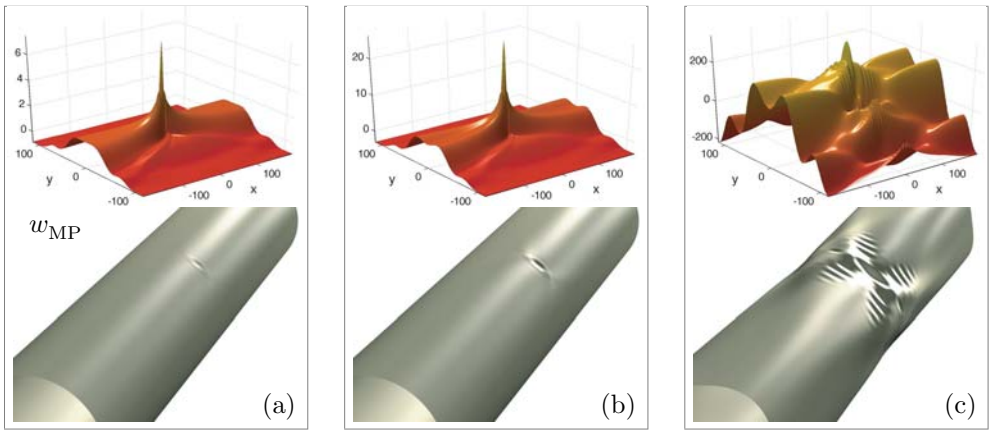

(a) $\dots V(\lambda) = F_\lambda(w_{\mathrm{MP}}) \approx 4.84$
(b) $\dots F_\lambda(w) \approx -15.57$
(c) $\dots F_\lambda(w) \approx -5.5 \cdot 10^4$

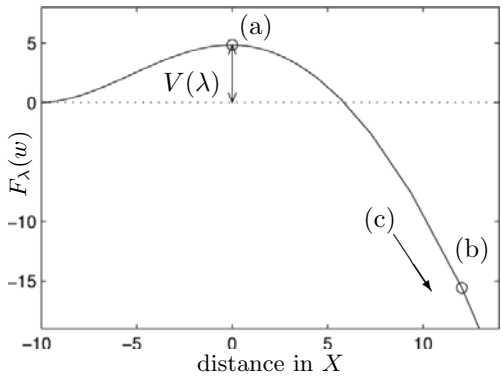

FIG. 1.3. *Part* (a) *shows a numerical computation of a solution* w_{MP} *that is a mountain pass point of the energy* F_λ *for a load* $\lambda = 1.5$. *We show the graph of the displacement* $w_{\mathrm{MP}}(x, y)$ *as a function of* (x, y) *as well as its rendering on a cylinder. At* w_{MP} *there exist two directions in the state space* X *in which the energy* F_λ *decreases. By perturbing* w_{MP} *in these directions and following a gradient flow of* F_λ, *we move away from* w_{MP}. *In one direction the dimple shrinks and disappears (not shown) and in the opposite its direction grows in amplitude and extent* ((b) *and* (c)).

is possible in the tangential direction has been an open problem for some time; it is interesting that our simulations for the perfect structure show solutions that are localized in both axial and tangential directions.

2. Like all mountain pass points, this single-dimple solution is unstable, in the sense that there are directions in state space in which the energy decreases. In one direction the dimple roughly shrinks and disappears, and in the opposite direction it grows and multiplies (Figures 1.3(b)–(c)). It is remarkable, however, that our numerical results indicate that the single-dimple solution has an alternative characterization as a *constrained global minimizer* (a global minimizer of the strain energy under prescribed end shortening).
3. The equations can be rescaled so that the only remaining parameters are the load level and the domain. The geometry of the mountain pass solution we calculate even appears to be independent of the domain size.

This mountain pass point is central in an estimate of the sensitivity to perturbations. For the system to escape from the neighborhood of the unbuckled state,

it must possess at least the energy associated with this mountain pass point. The mountain pass energy level is therefore an indication of the degree of stability of the unbuckled state. Implicitly it defines a class of perturbations for which the unbuckled state is stable. This approach is related to the "perturbation-energy" approach first suggested by Kröplin, Dinkler, and Hillmann [23], Duddeck et al. [11], and Wagenhuber and Duddeck [32], but differs in some essential points; see the discussion in section 5.

1.4. Methods. We use both analytical and numerical methods. In section 2 we introduce the von Kármán–Donnell equations, which form the basis of this paper, and rescale them in an appropriate manner. In section 3 we present the functional setting that we use, show that the energy functional has the geometry associated with a mountain pass, and prove the existence of mountain pass points (Lemma 3.6). There are certain interesting technical issues. By their localized nature, single-dimple solutions are most naturally defined on an unbounded domain; however, we are only able to prove existence of mountain pass points on bounded domains, and consequently we work on finite domains that become large in the limit of thin shells. Similarly, the noncoercive nature of the energy functional implies that we prove the existence of mountain pass points for almost all load levels (see Lemma 3.5).

In section 4 we turn to numerical investigation. We use a variety of different algorithms to find solutions of the discretized von Kármán–Donnell equations. With a discrete mountain pass algorithm we find solutions that are, by construction, mountain pass points. The solution of Figure 1.3(a) was found in this manner. With a constrained gradient flow we also find local minima of the strain energy under prescribed end shortening. Some of these solutions appear to coincide with those found by the discrete mountain pass algorithm, and the mountain pass solutions are stable under this gradient flow. These observations lead us to conjecture that the global mountain pass solution is also a global constrained minimizer of the strain energy. By a constrained version of the discrete mountain pass algorithm, we also find critical points of higher Morse index.

Section 5 is devoted to an interpretation of these results in the context of imperfection sensitivity, as mentioned above, and in section 6 we wrap up with the main conclusions.

2. The von Kármán–Donnell equations. We consider a cylindrical shell of radius R, thickness t, Young's modulus E, and Poisson's ratio ν that is subject to a compressive axial force P. In Appendix B we derive the dimensionless von Kármán–Donnell equations

$$\varepsilon^2\Delta^2\overline{w} + \bar{\lambda}\overline{w}_{xx} - \overline{\phi}_{xx} - 2[\overline{w},\overline{\phi}] = 0, \tag{2.1}$$

$$\Delta^2\overline{\phi} + [\overline{w},\overline{w}] + \overline{w}_{xx} = 0, \tag{2.2}$$

where subscripts x and y denote differentiation with respect to the spatial variables, the Laplacian Δ is given by $\Delta u = u_{xx} + u_{yy}$, and the bracket $[\cdot,\cdot]$ is defined as

$$[a,b] = \frac{1}{2}a_{xx}b_{yy} + \frac{1}{2}a_{yy}b_{xx} - a_{xy}b_{xy}.$$

The function $\overline{w}$ is the inward radial displacement measured from an unbuckled (fundamental) state, $\overline{\phi}$ is the Airy stress function, $\varepsilon^2 = t^2(192\pi^4R^2(1-\nu^2))^{-1}$, and the nondimensional load parameter is given by $\bar{\lambda} = P(8\pi^3ERt)^{-1}$. The unknowns $\overline{w}$ and $\overline{\phi}$ are defined on the two-dimensional spatial domain $(-\ell,\ell)\times(-1/2,1/2)$, where

$x \in (-\ell, \ell)$ is the axial and $y \in (-1/2, 1/2)$ is the tangential coordinate. Since the y-domain $(-1/2, 1/2)$ represents the circumference of the cylinder, the functions $\overline{w}$ and $\overline{\phi}$ are periodic in y; at the axial ends $x \in \{-\ell, \ell\}$ they satisfy the boundary conditions

$$\overline{w}_x = (\Delta \overline{w})_x = \overline{\phi}_x = (\Delta \overline{\phi})_x = 0.$$

For the experiments that we are interested in, the parameter ε is small, ranging from 10^{-2} to 10^{-4}. Here we rescale (2.1)–(2.2) such that the equations themselves are ε-independent, at the cost of a dependence on ε in the size of the spatial domain. Set

$$\overline{w} \mapsto \varepsilon w, \qquad \overline{\phi} \mapsto \varepsilon^2 \phi, \qquad x \mapsto \varepsilon^{1/2} x, \qquad y \mapsto \varepsilon^{1/2} y, \qquad \bar{\lambda} \mapsto \varepsilon \lambda, \tag{2.3}$$

so that the equations become

$$\Delta^2 w + \lambda w_{xx} - \phi_{xx} - 2\,[w, \phi] = 0, \tag{2.4}$$

$$\Delta^2 \phi + [w, w] + w_{xx} = 0. \tag{2.5}$$

The domain of definition of w and ϕ is now

$$\Omega := (-\ell \varepsilon^{-1/2}, \ell \varepsilon^{-1/2}) \times (-\tfrac{1}{2}\varepsilon^{-1/2}, \tfrac{1}{2}\varepsilon^{-1/2}),$$

which expands to $\mathbb{R}^2$ as $\varepsilon \to 0$. When not indicated otherwise, we choose the aspect ratio $2\ell = 1$; in section 4.3 we comment on the influence of domain size and aspect ratio.

The boundary conditions for w and ϕ now are

$$w \text{ is periodic in } y \quad \text{and} \quad w_x = (\Delta w)_x = 0 \text{ at } x = \pm \tfrac{1}{2}\varepsilon^{-1/2}, \tag{2.6a}$$

$$\phi \text{ is periodic in } y \quad \text{and} \quad \phi_x = (\Delta \phi)_x = 0 \text{ at } x = \pm \tfrac{1}{2}\varepsilon^{-1/2}. \tag{2.6b}$$

Equations (2.4)–(2.5) are related to the stored energy E and the average axial shortening S given by

$$E(w) := \frac{1}{2}\int_\Omega \left(\Delta w^2 + \Delta \phi^2\right) \qquad \text{and} \qquad S(w) := \frac{1}{2}\int_\Omega w_x^2. \tag{2.7}$$

Note that the function ϕ in (2.7) is determined from w by solving (2.5) with boundary conditions (2.6b); this uniquely defines ϕ up to an additive constant.

Solutions of (2.4)–(2.5) are stationary points of the total potential

$$F_\lambda(w) := E(w) - \lambda S(w). \tag{2.8}$$

This can be recognized as follows: If we substitute for w the perturbed function $w_\eta := w + \eta \tilde{w}$, then the perturbed Airy stress function ϕ_η solves

$$\Delta^2 \phi_\eta + [w, w] + 2\eta[w, \tilde{w}] + \eta^2 [\tilde{w}, \tilde{w}] + w_{xx} + \eta \tilde{w}_{xx} = 0.$$

Therefore $\phi_\eta = \phi + \eta \tilde{\phi} + O(\eta^2)$, where the perturbation $\tilde{\phi}$ solves

$$\Delta^2 \tilde{\phi} + 2[w, \tilde{w}] + \tilde{w}_{xx} = 0$$

with boundary condition (2.6b). Then

$$\begin{aligned} F'_\lambda(w)\cdot\tilde{w} &= \int_\Omega \Big[\Delta w\Delta\tilde{w} + \Delta\phi\Delta\tilde{\phi} - \lambda w_x\tilde{w}_x\Big] \\ &= \int_\Omega \Big[\Delta w\Delta\tilde{w} - \phi\big(2[w,\tilde{w}] + \tilde{w}_{xx}\big) - \lambda w_x\tilde{w}_x\Big] \\ &= \int_\Omega \Big[\Delta w\Delta\tilde{w} - \tilde{w}\big(2[w,\phi] + \phi_{xx}\big) - \lambda w_x\tilde{w}_x\Big], \end{aligned}$$

and this is a weak formulation of (2.4). Besides being stationary points of F_λ, solutions of (2.4)–(2.5) are also stationary points of E under the constraint of constant S; in this case λ is a Lagrange multiplier. We use both properties below.

3. The mountain pass: Overview. We briefly recall the general context of the Mountain Pass Theorem of Ambrosetti and Rabinowitz [2]. Let I be a functional defined on a Banach space X, and let w_1, w_2 be two distinct points in X. Consider the family Γ of all paths in X connecting w_1 and w_2 and define

$$c = \inf_{\gamma\in\Gamma}\max_{w\in\gamma} I(w), \tag{3.1}$$

that is, the infimum of the maxima of the functional I along paths in Γ. If $c > \max\{I(w_1), I(w_2)\}$, then the paths have to cross a "mountain range," and one may conjecture that there exists a critical point w_{MP} of I at the level c, called a mountain pass point.

We will apply this idea to the von Kármán–Donnell equations in the following way. We take for I the total potential F_λ (see (2.8)) at some fixed value of λ, and for the end point w_1 the origin. We will obtain a mountain pass solution by the following steps:

- MP1. We first show that $w_1 = 0$ is a strict local minimizer, or more precisely, that there exist $\varrho, \alpha > 0$ such that $F_\lambda(w) \geq \alpha$ for all w with $\|w\|_X = \varrho$ (Lemma 3.1).
- MP2. If ε is small enough, then there exists w_2 with $F_\lambda(w_2) \leq 0$ (Corollary 3.4).
- MP3. Given a sequence of paths γ_n that approximates the infimum in (3.1), we extract a (Palais–Smale) sequence of points $w_n \in \gamma_n$, each one close to the maximum along γ_n, and show that this sequence converges in an appropriate manner (Lemmas 3.5 and 3.6).

In this way it follows that there exists a mountain pass critical point w with $F_\lambda(w) = c$, provided that ε is sufficiently small (or that the domain is sufficiently large). For technical reasons (lack of coerciveness of the functional F_λ) this procedure can be performed only for almost all $0 < \lambda < 2$ (see Lemma 3.5).

In the rest of this section we detail the steps outlined above.

3.1. Choice of spatial domain. We are interested in mountain pass solutions of the system of equations (2.4)–(2.5) that are quasi independent of the domain size $\varepsilon^{-1/2}$, in the sense that they converge to a nontrivial solution on $\mathbb{R}^2$ as $\varepsilon \to 0$. This point of view suggests considering the problem on the whole of $\mathbb{R}^2$ rather than on a sequence of domains of increasing size; however, there are two reasons for not doing this. To start with, the numerical calculations described below are necessarily done on a bounded domain; more important, for the proof of existence of mountain pass points, boundedness of the domain is necessary. For these reasons we concentrate on bounded domains, while keeping the context of the unbounded domain in mind.

3.2. Functional setting and linearization. We introduce a functional setting for the functions w that is suggested by the linearization of the stored energy functional E. Writing $\phi = \phi_1 + \phi_2$, where

$$\Delta^2\phi_1 = -w_{xx} \qquad \text{and} \qquad \Delta^2\phi_2 = -[w,w], \tag{3.2}$$

we can expand the energy functional E as

$$E(w) = \frac{1}{2}\int_\Omega \Delta w^2 + \frac{1}{2}\int_\Omega \Delta\phi_1^2 + \int_\Omega \Delta\phi_1\Delta\phi_2 + \frac{1}{2}\int_\Omega \Delta\phi_2^2. \tag{3.3}$$

Since ϕ_2 is quadratic in w, the second derivative of E is given by

$$d^2E(0)\cdot u\cdot v = \int_\Omega \Delta u\Delta v + \int_\Omega \Delta\phi_1^u\Delta\phi_1^v,$$

where $\phi_1^{u,v}$ are obtained from u and v by replacing w with u or v in (3.2) and solving this equation for ϕ_1 with boundary conditions (2.6b). Inspired by this linearization of E, we define

$$X = \left\{\psi \in H^2(\Omega) : \psi_x\left(\pm\frac{1}{2}\varepsilon^{-1/2},\cdot\right) = 0,\ \psi \text{ is periodic in } y, \text{ and } \int_\Omega \psi = 0\right\}$$

with norm

$$\|w\|_X^2 = \int_\Omega \big(\,\Delta w^2 + \Delta\phi_1^2\,\big),$$

where $\phi_1 \in H^2(\Omega)$ is the unique solution of

$$\Delta^2\phi_1 = -w_{xx}, \qquad \phi_1 \text{ satisfies (2.6b)}, \qquad \text{and} \qquad \int_\Omega \phi_1 = 0.$$

This norm is equivalent to the H^2-norm on the set X, and with the appropriate inner product the space X is a Hilbert space.

We now address the requirements of the mountain pass theorem mentioned above in MP1–MP3.

3.3. The origin is a local minimizer. The norm in X is related in a natural manner to the shortening S, as demonstrated by the (sharp) estimate

$$\begin{aligned} 2S(w) &= \int_\Omega w_x^2 = -\int_\Omega w w_{xx} = \int_\Omega w\Delta^2\phi_1 \\ &= \int_\Omega \Delta w\Delta\phi_1 \le \frac{1}{2}\int_\Omega \Delta w^2 + \frac{1}{2}\int_\Omega \Delta\phi_1^2 = \frac{1}{2}\|w\|_X^2\,. \end{aligned} \tag{3.4}$$

This inequality strongly suggests that for $\lambda < 2$ the origin is a strict local minimum for the functional $F_\lambda(w) = E(w) - \lambda S(w)$.

LEMMA 3.1. *For any $\lambda < 2$, there exists $\varrho > 0$ such that*

$$\inf\big\{\ F_\lambda(w) : \|w\|_X = \varrho\ \big\} > 0.$$

Proof. Split $\phi = \phi_1 + \phi_2$ as in (3.2), and note that the function $\nabla\phi_1$ is bounded in L^∞ by the Sobolev imbedding $\{\psi \in H^3 : \int\psi = 0\} \hookrightarrow L^\infty$:

$$\|\nabla\phi_1\|_{L^\infty}^2 \le C\left\|\Delta^2\phi_1\right\|_{L^2}^2 = C\|w_{xx}\|_{L^2}^2\,.$$

The third term on the right-hand side of (3.3) can now be rewritten as

$$\int_\Omega \Delta\phi_1\Delta\phi_2 = \int_\Omega \phi_1[w,w] = \int_\Omega \phi_1(w_{xx}w_{yy} - w_{xy}^2) = \int_\Omega (\phi_{1y}w_x w_{xy} - \phi_{1x}w_x w_{yy}),$$

which we estimate by

$$\left|\int_\Omega \Delta\phi_1\Delta\phi_2\right| \le 2\,\|\nabla\phi_1\|_{L^\infty}\,\|w_x\|_{L^2}\,\|\Delta w\|_{L^2} \le C\,\|w_x\|_{L^2}\,\|\Delta w\|_{L^2}^2 \le C\sqrt{S(w)}\,\|w\|_X^2\,.$$

Since $\lambda < 2$, choose $0 < \varrho < (2-\lambda)/2C$ and define $\eta = (1/2)(1 - C\varrho - \lambda/2) > 0$. Then on the set $\mathcal{C} = \{w : \|w\|_X = \varrho\}$, using (3.4), we find that

$$\begin{aligned} F_\lambda(w) &= E(w) - \lambda S(w) \\ &\ge \frac{1}{2}\,\|w\|_X^2 - C\sqrt{S(w)}\,\|w\|_X^2 - \lambda S(w) \\ &\ge \frac{\varrho^2}{2} - C\varrho^3\frac{1}{2} - \lambda\frac{\varrho^2}{4} \\ &= \frac{\varrho^2}{2}\left(1 - C\varrho - \frac{\lambda}{2}\right) \\ &= \eta\varrho^2. \qquad \square \end{aligned}$$

This lemma implies that by choosing w_1 to be the origin we have shown condition MP1.

Remark 3.2. Although inequality (3.4) suggests that the origin should be a local minimizer for any domain Ω, bounded or not, the proof above applies only to bounded domains. F. Otto has constructed a proof of this result that is valid on any domain (private communication). Interestingly, this proof uses not only the cubic energy term $\int_\Omega \Delta\phi_1\Delta\phi_2$, but also the quartic term $\int_\Omega \Delta\phi_2^2$, and appears to break down without this latter term.

3.4. Periodic solutions exist with negative F_λ. To satisfy MP2 we show in this section that for any $\lambda > 0$, functions $w \in X$ exist, for which $F_\lambda(w) = E(w) - \lambda S(w) < 0$. To do this we construct a sequence of functions w_δ with specific scaling properties.

LEMMA 3.3. *There exists a sequence of functions w_δ, 1-periodic on $\mathbb{R}^2$, such that as $\delta \to 0$,*

1. $\displaystyle\int_{[-1/2,1/2]^2} w_{\delta x}^2 \longrightarrow c \quad$ *for some $c > 0$,*
2. $\displaystyle\int_{[-1/2,1/2]^2} \Delta w_\delta^2 = O(\delta^{-1})$

   and $\displaystyle\int_{[-1/2,1/2]^2} \Delta\phi_\delta^2 = O(\delta^{2-\alpha}) \quad$ *for any $\alpha > 0$.*

Here the functions w_δ and ϕ_δ solve (2.5) *with periodic boundary conditions. In addition, w_δ and ϕ_δ satisfy boundary conditions* (2.6) *on the boundary of $[-1/2,1/2]^2$.*

The proof, given in Appendix A, is inspired by the so-called *Yoshimura pattern* [37], a folding pattern by which a flat sheet of paper, or a cylindrical sheet of thin material, can be folded into a macroscopically cylindrical structure with zero Gaussian curvature but locally infinite total curvature (Figure 3.1). The functions w_δ are smoothed versions of the Yoshimura pattern, adapted to the geometrically

FIG. 3.1. *Yoshimura folding pattern.*

linear setting of the von Kármán–Donnell equations, and δ measures the width of the fold.

COROLLARY 3.4.

1. *Fix $\lambda > 0$. If ε is sufficiently small, then there exists $w \in X$ such that $F_\lambda(w) < 0$.*
2. *Fix ε sufficiently small. Then there exists $\lambda_0(\varepsilon) \in [0, 2)$ such that for all $\lambda > \lambda_0$, there exists $w \in X$ with $F_\lambda(w) < 0$.*

Proof. By scaling the functions w_δ of Lemma 3.3, the claims can be fulfilled as follows: Let $\delta = \varepsilon^{2/3}$, and set

$$\tilde{w}_\varepsilon(x, y) = \varepsilon^{-1} w_{\varepsilon^{2/3}}(x\varepsilon^{1/2}, y\varepsilon^{1/2}), \qquad \tilde{\phi}_\varepsilon(x, y) = \varepsilon^{-2}\phi_{\varepsilon^{2/3}}(x\varepsilon^{1/2}, y\varepsilon^{1/2});$$

then $\tilde{w}_\varepsilon \in X$, and (2.5) is invariant under this scaling; in addition, choosing $\alpha = 1/6$, we obtain

$$Q_\varepsilon := \frac{\displaystyle\int_{\Omega_\varepsilon} \left[\Delta\tilde{w}_\varepsilon^2 + \Delta\tilde{\phi}_\varepsilon^2\right]}{\displaystyle\int_{\Omega_\varepsilon} \tilde{w}_{\varepsilon x}^2} = O\big(\varepsilon^{1/6}\big) \qquad \text{as } \varepsilon \to 0.$$

Therefore $\lim_{\varepsilon\to 0} Q_\varepsilon = 0$, proving the first claim. For the second claim, we fix ε such that $Q_\varepsilon < 2$; then for all $\lambda > Q_\varepsilon$, $F_\lambda(\tilde{w}_\varepsilon) < 0$. ∎

3.5. Convergence of selected sequences. For given $\lambda \in (0, 2)$ and for sufficiently small $\varepsilon > 0$, the two previous sections provide two points: the origin $w_1 = 0$ that satisfies MP1, and a point w_2 with $F_\lambda(w_2) < 0$, such that

$$c(\lambda) := \inf_{\gamma\in\Gamma} \max_{w\in\gamma} F_\lambda(w) > 0, \tag{3.5}$$

where Γ is the set of curves connecting 0 and w_2,

$$\Gamma = \{\gamma \in C([0, 1]; X) : \gamma(0) = 0,\ \gamma(1) = w_2\}$$

(actually, Γ depends on λ through the dependence on w_2, but w_2 can be taken independently of λ in a neighborhood of a given $\lambda \in (0, 2)$).

We were unable to prove the classical Palais–Smale condition, which reads as follows:

> For any sequence $w_n \in X$ such that $F_\lambda(w_n) \to c$ and $F'_\lambda(w_n) \to 0$ in X', there exists a subsequence that converges in X.

The difficulty lies in the lack of coerciveness of the functional F_λ: the quotient $F_\lambda(w)/\|w\|_X^2$ is not bounded away from zero, implying that Palais–Smale sequences may be unbounded in X.

The "Struwe monotonicity trick" [29] provides a way of proving the boundedness of Palais–Smale sequences for at least *almost all* $\lambda \in (0,2)$. The pertinent observation is that for fixed w, $F_\lambda(w)$ is decreasing in λ; consequently, $c(\lambda)$ is a decreasing function of λ and therefore differentiable in almost all $\lambda \in (0,2)$. If $\gamma(t)$ is the highest point of a near-optimal curve γ at some λ_0, then $c'(\lambda_0)$ should be close to $-S(\gamma(t))$. Finiteness of c' at λ_0 thus implies that near–mountain pass points have bounded S, and this additional information suffices for the construction of bounded sequences.

LEMMA 3.5. *Let $\lambda \in (0,2)$ be such that $c'(\lambda)$ exists. Then there exists a bounded Palais–Smale sequence w_n, i.e., a sequence satisfying that*

1. *w_n is bounded in X;*
2. *$F'_\lambda(w_n) \to 0$ in X' and $F_\lambda(w_n) \to c(\lambda)$;*
3. *there exists a sequence of curves $(\gamma_n) \subset \Gamma$ such that $w_n \in \gamma_n([0,1])$ and $\max_{t\in[0,1]} F_\lambda(\gamma_n(t)) \to c(\lambda)$.*

In [28] this same argument was used to study mountain pass points for the related one-dimensional functional

$$J_\lambda(u) = \int_{\mathbb{R}} \Big\{ \frac{1}{2} u''^2 - \frac{\lambda}{2} u'^2 + F(u) \Big\},$$

where F is a nonnegative double- or single-well potential. The proof of Lemma 3.5 repeats verbatim the proof of [28, Prop. 5], and we omit it here.

LEMMA 3.6. *The sequence w_n given by Lemma 3.5 is compact in X, and a subsequence converges to a stationary point $w \in X$ of F_λ.*

Strictly speaking, the stationary point given by this lemma may not be a mountain pass point itself, in the sense that there may not be a curve $\gamma \in \Gamma$ of which w is the highest point. Property 3 of Lemma 3.5, however, states that w has an approximate mountain pass character.

Proof. We extract a subsequence that converges weakly in X and strongly in H^1 and L^∞ to a limit w. Defining ϕ_{1n} and ϕ_{2n} by (3.2), we find that the right-hand sides in (3.2) are bounded in L^2 and L^1, and therefore that ϕ_{1n} and ϕ_{2n} converge strongly (up to extracting a subsequence, which we do without changing notation) in H^2 to functions $\phi_{1,2}$. Both functions $\phi_{1,2}$ are again related to w by (3.2); for ϕ_2 this follows from remarking that for given $\zeta \in C_c^\infty(\Omega)$,

$$\lim_{n\to\infty} \int_\Omega \zeta[w_n, w_n] = \lim_{n\to\infty} \int_\Omega w_n[\zeta, w_n] = \int_\Omega w[\zeta, w] = \int_\Omega \zeta[w, w],$$

so that the right-hand side converges in the sense of distributions. Similarly, it follows from the strong H^2-convergence of $\phi_n = \phi_{1n} + \phi_{2n}$ that

$$\lim_{n\to\infty} \int_\Omega \phi_n[w_n, w - w_n] = \lim_{n\to\infty} \int_\Omega w_n[\phi_n, w - w_n] = 0.$$

To show that w_n converges strongly in X, note that the derivative $F'_\lambda(w_n)$ can be characterized as

$$F'_\lambda(w_n) \cdot v = \int_\Omega \Delta w_n \Delta v - \int_\Omega \phi_n\big(v_{xx} + 2[w_n, v]\big) - \lambda \int_\Omega w_{nx} v_x.$$

We now calculate

$$\lim_{n\to\infty}\left\{\int_\Omega \Delta w^2 - \int_\Omega \Delta w_n^2\right\} = \lim_{n\to\infty}\int_\Omega \Delta w_n \Delta(w-w_n)$$
$$= \lim_{n\to\infty}\left\{F_\lambda'(w_n)\cdot(w-w_n) + \int_\Omega \phi_n\big((w-w_n)_{xx} + 2[w_n, w-w_n]\big) + \lambda\int_\Omega w_{nx}(w-w_n)_x\right\} = 0.$$

The strong convergence of w_n in X now follows from the uniform convexity of X. ∎

4. Numerical results.

4.1. Description of the algorithm. Our goal in this section is to find, numerically, critical points of F_λ. Although we will focus on mountain pass points described above and sketch the method used to find them, numerical approximations of other critical points of F_λ will be shown as well. More details on all the numerical methods used are given in a companion paper [17].

In order to employ the mountain pass algorithm, we discretize (2.4)–(2.8) using finite differences. The algorithm was first proposed in [8] for a second-order elliptic problem in one dimension. It was later used in [18] for a fourth-order problem in two dimensions.

The main idea of the algorithm is illustrated in Figure 4.1. We take a discretized path connecting $w_1 = 0$ with a point w_2 such that $F_\lambda(w_2) < 0$. After finding the point z_m at which F_λ is maximal along the path, this point is moved a small distance in the direction of the steepest descent of F_λ. Thus the path has been deformed and the maximum of F_λ lowered. This deforming of the path is repeated until the maximum along the path cannot be lowered any more: a critical point w_{MP} has been reached.

Figure 4.2(a) shows a numerical solution of (2.4)–(2.5) obtained by this algorithm with $\lambda = 1.1$. The graph in each panel shows the radial displacement w as a function

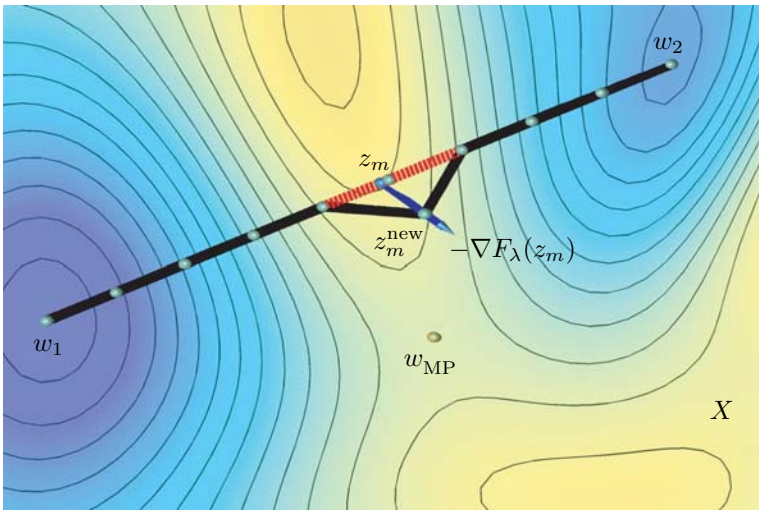

FIG. 4.1. *Deforming the path in the main loop of the mountain pass algorithm: point z_m is moved a small distance in the direction $-\nabla F_\lambda(z_m)$ and becomes z_m^{new}. This step is repeated until the mountain pass point w_{MP} is reached.*

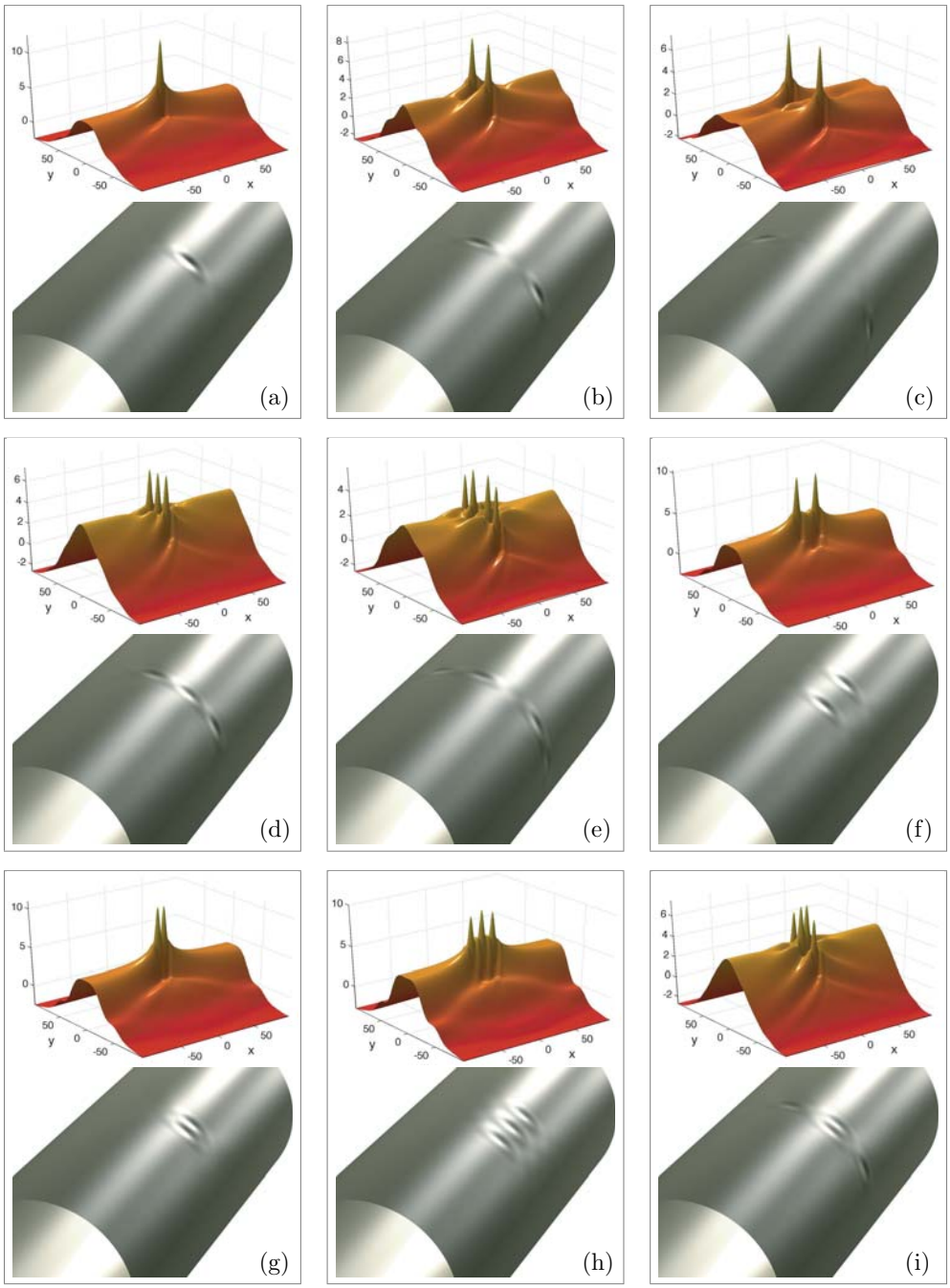

FIG. 4.2. *Numerical solutions found using the (constrained) mountain pass algorithm, constrained steepest descent method, and the Newton algorithm. The figures show both the graph of* $w(x, y)$ *and its rendering on a cylinder.*

of x and y. Rendered on a cylinder, this solution represents a single dimple, as can be seen below the graphs.

We restrict our computations to functions that are even about the x- and y-axes, i.e., to the subspace

$$\mathscr{S} = \{\psi \in X : \psi(x,y) = \psi(-x,y),\ \psi(x,y) = \psi(x,-y)\},$$

thus reducing the computational domain Ω to one quarter, e.g., $(0, \frac{1}{2}\varepsilon^{-1/2})\times(0, \frac{1}{2}\varepsilon^{-1/2})$. The boundary conditions (2.6a) then become

$$w_x = (\Delta w)_x = 0 \text{ for } x \in \{0, \tfrac{1}{2}\varepsilon^{-1/2}\} \quad \text{and} \quad w_y = (\Delta w)_y = 0 \text{ for } y \in \{0, \tfrac{1}{2}\varepsilon^{-1/2}\}.$$

This symmetry assumption has many numerical advantages, but on the other hand it a priori excludes solutions that do not belong to $\mathscr{S}$.

For the mountain pass algorithm, we always use the unbuckled state $w_1 = 0$ as the first end point of the paths. The choice of the second end point w_2 has a nontrivial influence on the solution to which the mountain pass algorithm converges. Corollary 3.4 guarantees the existence of $w_2 \in \mathscr{S}$ with $F_\lambda(w_2) < 0$; in the numerical implementation, however, we found such a w_2 by a steepest descent method (rather than by taking the function constructed in the proof of Lemma 3.3): starting from a function w_0 that has one peak located in the center of the domain Ω, we solved the initial value problem

$$\frac{d}{dt}w(t) = -\nabla F_\lambda(w(t)), \quad w(0) = w_0, \tag{4.1}$$

on an interval $(0,T)$ until $F_\lambda(w(T)) < 0$. We then defined $w_2 = w(T)$.

A different choice of w_2 (or, more precisely, of the starting point w_0 of (4.1)) can lead to a different solution of the problem, as Figures 4.2(b) and (f) show. Here w_0 was chosen to have two peaks with centers on the axes $x = 0$ and $y = 0$, respectively. The algorithm then converged to a numerical solution with two dimples in the circumferential and axial directions, respectively.

Note that the numerical solution w_{MP} selected by the mountain pass algorithm has the mountain pass property in a certain neighborhood only: there exists a ball $B_\rho(w_{\mathrm{MP}})$ and two points $\tilde{w}_1, \tilde{w}_2 \in B_\rho(w_{\mathrm{MP}})$ such that

$$F_\lambda(w_{\mathrm{MP}}) = \inf_{\gamma\in\tilde{\Gamma}} \max_{w\in\gamma} F_\lambda(w) > \max\{F_\lambda(\tilde{w}_1), F_\lambda(\tilde{w}_2)\},$$

where $\tilde{\Gamma}$ is the set of curves in $B_\rho(w_{\mathrm{MP}})$ connecting $\tilde{w}_1$ and $\tilde{w}_2$. The reason for this is that the algorithm deforms a certain initial path connecting w_1 and w_2 which is fixed. In order to recover the global character, one would need to run the algorithm for all possible initial paths.

The rest of the numerical solutions shown in Figure 4.2 were obtained under a prescribed value of shortening S by the constrained steepest descent method and the constrained mountain pass algorithm [16, 17].

4.2. Calculation of $F_\lambda(w_{\mathrm{MP}})$. In the preceding sections we showed that

1. for a sufficiently large domain Ω, a function w_2 on Ω exists with $F_\lambda(w_2) < 0$;
2. for each such function w_2 and for almost all $0 < \lambda < 2$, a mountain pass solution $w_{\mathrm{MP}} = w_{\mathrm{MP}}(\lambda, \Omega, w_2)$ exists.

Different end points w_2 may give rise to different mountain pass points, as we have observed in the numerical experiments described above. We therefore define the mountain pass energy function V on $(0,2)$ by

$$V(\lambda,\Omega) := \inf_{w_2}\{\, F_\lambda\big(w_{\mathrm{MP}}(\lambda,\Omega,w_2)\big) : F_\lambda(w_2) < 0\,\}. \tag{4.2}$$

For a given λ, the value of $V(\lambda,\Omega)$ is the lowest height (or energy level) at which one may pass from the origin to a point with negative total potential F_λ. We now derive some of its properties and calculate it numerically.

LEMMA 4.1 (properties of $V(\lambda,\Omega)$).

1. *For sufficiently large Ω there exists $\lambda_0(\Omega) \geq 0$ such that $V(\lambda,\Omega) < \infty$ for almost all $\lambda \in (\lambda_0, 2)$.*
2. *V is a decreasing function of λ.*
3. *For sufficiently large Ω, there exists $c(\Omega) > 0$ such that*

$$V(\lambda,\Omega) \leq c(2-\lambda)^3$$

for sufficiently small $2-\lambda > 0$.

Proof. Part 1 is a reformulation of the main result of section 3, making use of Corollary 3.4. For part 2 we remark that for each fixed w, $F_\lambda(w)$ is a decreasing function of λ; the infimum of a set of decreasing functions is again decreasing.

For part 3, let us set

$$E(w) = E_2(w) + E_3(w) + E_4(w),$$

where

$$E_2(w) := \frac{1}{2}\,\|w\|_X^2 = \frac{1}{2}\int_\Omega \big(\Delta w^2 + \Delta\phi_1^2\big), \quad E_3(w) := \int_\Omega \Delta\phi_1\Delta\phi_2,$$
$$\text{and} \quad E_4(w) := \frac{1}{2}\int_\Omega \Delta\phi_2^2,$$

where ϕ_1 and ϕ_2 are determined from w by (3.2) (see also (3.3)). Note that E_n has homogeneity n, i.e., $E_n(\mu w) = \mu^n E_n(w)$.

A classical result in the engineering literature of cylinder buckling (see, e.g., [20]) states that there exists a periodic function w on $\mathbb{R}^2$ such that

$$E_2(w) = 2S(w) \qquad \text{and} \qquad E_3(w) + E_4(w) < 0.$$

Here and below we consider the integrals that define $E_n(w)$ and $S(w)$ as taken over a single period cell. For sufficiently small $2-\lambda > 0$ the inequality above gives that $F_\lambda(w) = (2-\lambda)S(w) + E_3(w) + E_4(w)$ is negative, implying that w is an admissible end point w_2 for definition (4.2) of $V(\lambda,\Omega)$, and the connecting line segment $\{\mu w : 0 \leq \mu \leq 1\}$ is therefore an admissible curve in Γ. Consequently,

$$V(\lambda) \leq \sup_{0\leq\mu\leq 1} F_\lambda(\mu w) = \sup_{0\leq\mu\leq 1} \mu^2(2-\lambda)S(w) + \mu^3 E_3(w) + \mu^4 E_4(w).$$

The supremum on the right-hand side is obtained at

$$\mu = \frac{3\,|E_3(w)|}{8E_4(w)}\left\{1 - \sqrt{1 - \frac{32(2-\lambda)S(w)E_4(w)}{9E_3(w)^2}}\right\}$$
$$= \frac{2S(w)}{3\,|E_3(w)|}\,(2-\lambda) + o(1) \quad \text{as } \lambda \to 2,$$

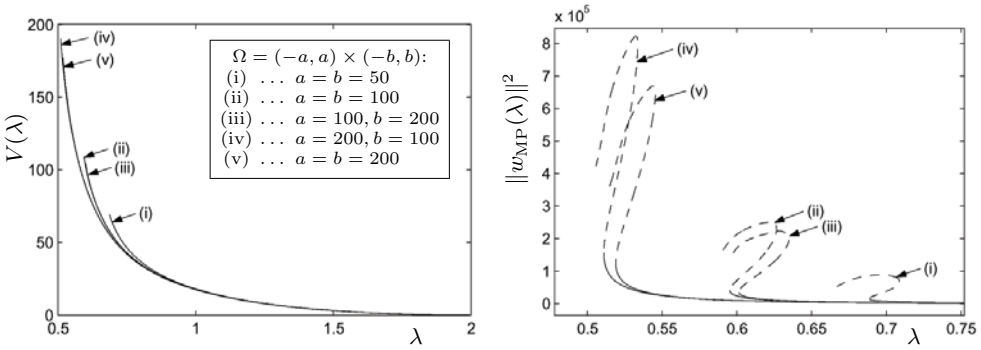

FIG. 4.3. *Left: The mountain pass energy $V(\lambda, \Omega)$ found numerically for various sizes of domain Ω. Right: The solid line shows the same computation as on the left, but plotted for the norm of $w_{\mathrm{MP}}(\lambda)$ squared. The dashed curve was obtained by continuation of the solid curve; the solutions on the dashed curve do not represent mountain pass points.*

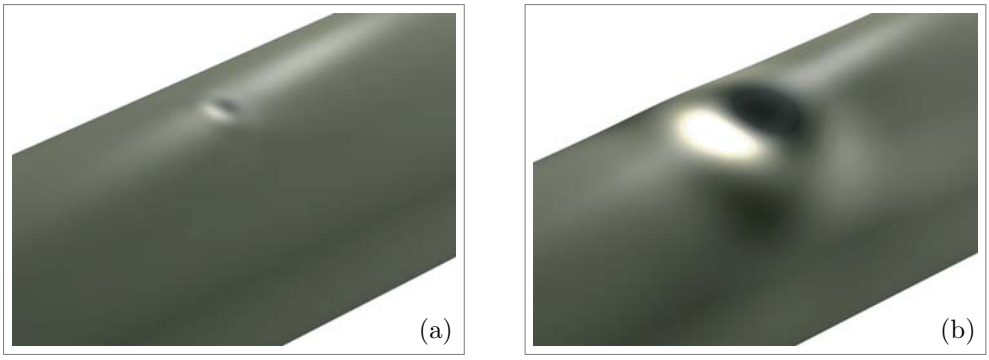

FIG. 4.4. *The numerical mountain pass solution w_{MP} of the scaled equations* (2.4)–(2.5) *for a given value of λ rendered on two cylinders of the same radius R but a different thickness t:* (a) $t/R = 0.003$, (b) $t/R = 0.04$.

implying that the claim holds for periodic functions. The generalization to nonperiodic functions on large domains Ω (i.e., for small ε) is made by filling the domain with a large number of periodic cells of the function w and connecting the function smoothly to the boundary of Ω. □

Figure 4.3 shows graphs of the mountain pass energy $V(\lambda, \Omega)$ computed for various sizes of domain Ω. For each domain, the mountain pass algorithm was employed to compute w_{MP} for several values of λ. These mountain pass solutions were then continued in λ using numerical path following.

4.3. Influence of the domain. The localized nature of the solutions calculated above suggests that they should be independent of domain size, in the sense that for a sequence of domains of increasing size the solutions converge (for instance, pointwise on compact subsets). Such a convergence would also imply convergence of the associated energy levels. Similarly, we would expect that the aspect ratio of the domain is of little importance in the limit of large domains.

We have tested these hypotheses by computing mountain pass solutions on domains of different sizes and aspect ratios. Generally solutions on different domains compare well; the maximal difference between the second derivatives of w is two or

three orders of magnitude smaller than the supremum norm of the same derivative (the details of this comparison are given in [17]).

Here we include only a calculation of the mountain pass energy level $V(\lambda, \Omega)$ for different aspect ratios and sizes of domain Ω (see Figure 4.3).

The comparison of solutions computed on different domains and their respective energies suggests that for each λ we are indeed dealing with a single, localized function defined on $\mathbb{R}^2$, of which our computed solutions are finite-domain adaptations. In the rest of this paper we adopt this point of view, and consequently we will write $V(\lambda)$ instead of $V(\lambda, \Omega)$.

A consequence of this point of view is that dimples in cylinders with different geometric parameters are mapped to the same rescaled solution, or equivalently, that the same single-dimple solution of (2.4)–(2.5) corresponds to differently sized dimples on an actual cylinder, as a function of the parameters (see Figure 4.4).

5. Interpretation: Imperfection sensitivity. We now turn to the relevance of the mountain pass in the context of a loading problem. This relevance can be best understood in the context of imperfections in the loading conditions (rather than geometric imperfections) such as in the case of a (small) lateral loading.

Under a small lateral load, an equilibrium w_0, which is a local minimum of the functional F_λ, may be perturbed into an equilibrium $\tilde{w}_0$ of a perturbed functional $\tilde{F}_\lambda$. Since w_0 is a local minimum, $F_\lambda(\tilde{w}_0) > F_\lambda(w_0)$; i.e., with respect to the unperturbed system, $\tilde{w}_0$ has a higher total potential than w_0. The level of F_λ that is reached is a measure of the magnitude of the imperfection—a different measure than is commonly used, but one that has distinct advantages.

By definition, the number $V(\lambda)$ is the lowest energy level at which it is possible to move between the basins of attraction of w_1 and w_2 (Figure 5.1). If the loading imperfection is interpreted, as above, as a mechanism capable of maintaining the system at a higher energy level than that of the neighboring fundamental minimizer, then the number $V(\lambda)$ is critical: as long as the imperfection is so small that the energy is never raised by more than $V(\lambda)$, the new stationary point will be part of the same basin of attraction as w_1. For larger imperfections, however, it becomes possible to leave the fundamental basin of attraction, resulting in a large jump in state space.

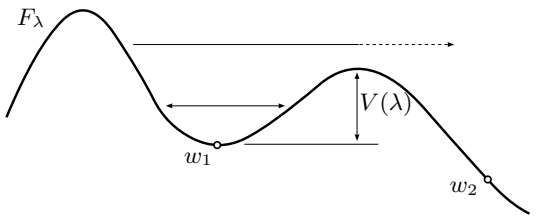

FIG. 5.1. *In order to leave the basin of attraction of w_1, the surplus energy should exceed $V(\lambda)$.*

This line of reasoning provides a natural measure of the size of imperfections, namely, the maximal increase in energy (in the perfect structure) that an imperfection can achieve. It also provides a natural measure of the stability of the unbuckled state, since a higher mountain pass energy level implies a larger class of loading imperfections under which the state remains in the fundamental basin of attraction. This observation allows us to connect systems with different geometrical characteristics and compare their relative sensitivity to imperfections.

5.1. Calibrating the mountain pass energy. Comparing cylinders of varying geometries requires a common measure of imperfection sensitivity. It is not a priori clear which measure to take; e.g., one might consider either the mountain pass energy itself or the average spatial density of this energy, which will result in different comparisons for cylinders of different wall volumes. Here we choose to rescale the mountain pass energy level by the other energy level present in the loaded cylinder, i.e., the energy that is stored in the homogeneous compression of the unbuckled shell.

This calculation can be done in two slightly different ways. The first and most straightforward is to rescale the dimensional mountain pass energy (see (B.11) and (2.3)),

$$64\pi^6 EtR^2\varepsilon^3 V(\lambda) = \frac{Et^4}{8(3(1-\nu^2))^{3/2}R}\, V(\lambda),$$

by the elastic strain energy stored in the full length of the compressed cylinder of length L,

$$\frac{L}{4\pi ERt}\, P^2 = \frac{\pi t^3 EL}{12(1-\nu^2)R}\, \lambda^2,$$

to give an energy ratio, or a rescaled mountain pass energy level,

$$\alpha = \frac{1}{2\pi\sqrt{3(1-\nu^2)}}\, \frac{t}{L}\, \frac{V(\lambda)}{\lambda^2}. \tag{5.1}$$

From this expression and the calculation shown in Figure 4.3, curves may be drawn in a plot of load versus the ratio L/t (see Figure 5.2). Note that to obtain this figure from Figure 4.3 the curve $V(\lambda)$ was fitted to extend the range of λ. Figure 5.2 shows the following two remarkable features:

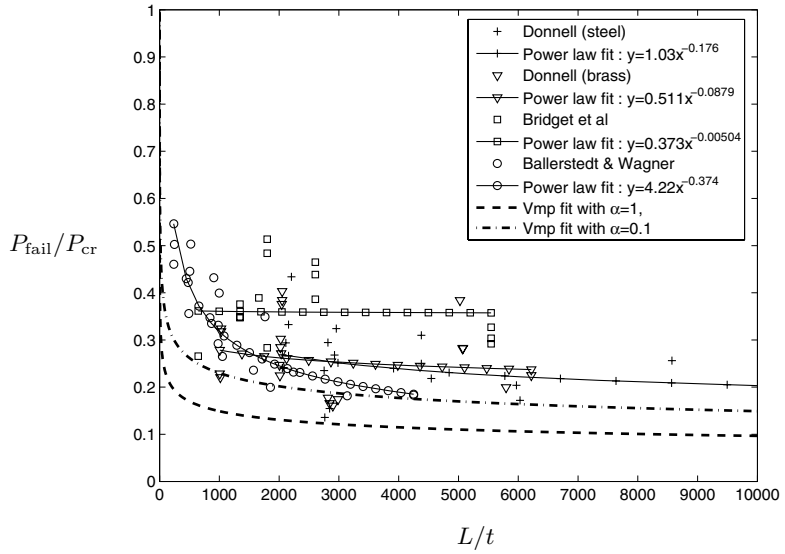

FIG. 5.2. *Shown are the same data as in Figure* 1.1*, with the addition of two curves of constant* $\alpha = 1$*,* $\alpha = 0.1$*, where* α *is given in* (5.1)*. Note that the load at which the mountain pass energy equals the stored energy in the prebuckled cylinder* ($\alpha = 1$) *appears to be a lower bound on the data.*

1. The general trend of the constant-α curves is very similar to the trend of the experimental data.
2. The $\alpha = 1$ curve, which indicates the load at which the mountain pass energy equals the stored energy in the prebuckled cylinder, appears to be a lower bound on the data.

One may also consider an alternative way of rescaling energy. The cylinder is a long structure, and it is not clear to what extent the length of the structure is relevant for the imperfection sensitivity. It may be reasonable to compare the energy of the mountain pass with the stored energy contained in a representative section of the cylinder; the radius R provides a natural length scale for such a representative section.

Similar to Figure 5.2, Figure 5.3 presents curves of constant β, where β is the ratio of mountain pass energy to stored energy in a section of length $2\pi R$:

$$\beta = \frac{1}{4\pi^2\sqrt{3(1-\nu^2)}}\,\frac{t}{R}\,\frac{V(\lambda)}{\lambda^2}. \tag{5.2}$$

Once again, to obtain Figure 5.3 we fitted $V(\lambda)$ from Figure 4.3 to extend the range of λ.

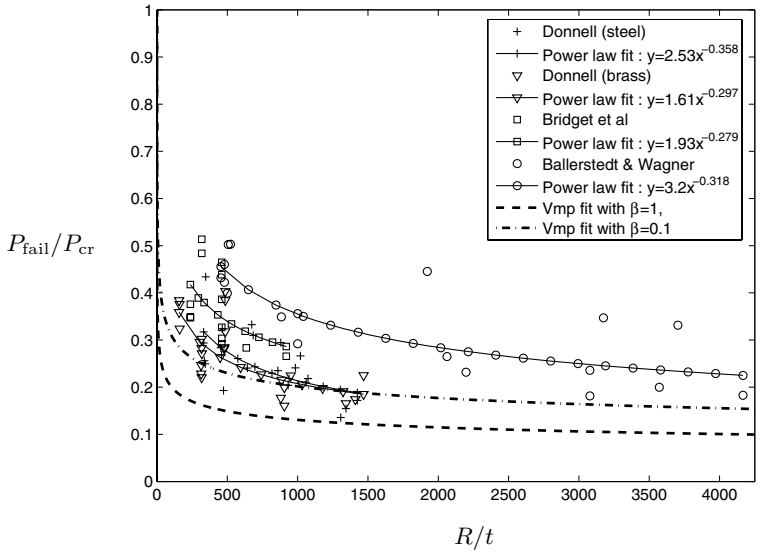

FIG. 5.3. *Experimental data and fit to V_{mp} with $\beta = 1$ and $\beta = 0.1$ in (5.2). Again, the load at which the mountain pass energy equals the stored energy in a representative portion of the prebuckled cylinder ($\beta = 1$) appears to be a lower bound on the data.*

6. Discussion and conclusions. The mathematical results and their interpretation in the context of a loading problem have brought about a number of new and improved insights.

6.1. The cylinder has doubly localized solutions. The subcritical nature of the bifurcation in Figure 1.2 strongly suggests that equilibria exist with deformation localized to a small portion of the cylinder length. In [20, 24, 25] such solutions are indeed calculated numerically and investigated analytically; these solutions are periodic around the cylinder and have exponential decay in the axial direction.

The localization in the axial direction demonstrated by these solutions is consistent with results on simpler systems, such as the laterally supported strut [21, 26]. The behavior of the cylinder in the tangential direction is not as well understood. The lack of localization in the simply supported flat plate [13] suggests that the cylinder should also prefer tangentially delocalized solutions, as do most of the experiments. The single- and multiple-dimple solutions of this paper, however, clearly demonstrate that doubly localized solutions do exist, and that some of these can be stable under constrained shortening.

6.2. The mountain pass is a single-dimple solution. The fact that the mountain pass solution exists follows essentially from two features, the local minimality of the unbuckled state and the existence of a large-deflection state of lower energy. The former is a simple consequence[3] of the subcritical load level, but the latter is based on an essential property of the cylinder: for a sequence of cylinders for which $R/t \to \infty$, the nondimensionalized load-carrying capacity (the highest load at which the unbuckled state is not only a local but also a global energy minimizer) decreases to zero. This property was demonstrated implicitly by Hoff, Madsen, and Mayers [15], and Lemma 3.3 provides a simplified proof of this result and a simple sequence of functions that illustrates the property.

However, the fact that the mountain pass solution is localized, and even is the most localized solution that is possible—a single dimple—is interesting in its own right and provides a complementary view of the discussion of localization above. A different way of formulating this result is that "creating the first dimple is the major obstacle"; afterwards one may increase the size of the dimple and add further dimples without ever returning to the same high energy level. In itself this interpretation points to a relationship between single dimples and imperfection sensitivity.

6.3. Single dimples in other contexts. Interestingly, single dimples have appeared in the literature in a number of seemingly unrelated ways:

- In the celebrated high-speed camera images of Eßlinger [12], the first visible deformation is a single, well-developed dimple halfway between the ends of the cylinder. New dimples quickly appear next to this first dimple, and the deformation then spreads around the cylinder in an axial direction. It is remarkable, though, that the first visible deformation is a single dimple.
- Some of the "worst" imperfections calculated by Deml and Wunderlich [9] and Wunderlich and Albertin [35] are in the form of a single dimple; as the load decreases, the dimple contracts and becomes even more concentrated.
- Hühne et al. [19] assert that single dimples are also *realistic* and *stimulating* imperfections in the sense of [34].
- Zhu, Mandal, and Calladine [38] base their analysis of the scaling behavior of the experimental buckling load on the behavior of a single dimple in other structural situations (such as the point-loaded cylinder and the sphere under uniform external pressure).

Note that the single-dimple appearances above are of three different types. Eßlinger's dimple is an experimental observation; the dimples of Wunderlich and coworkers and of Hühne et al. are geometric imperfection profiles; and the dimples studied by Zhu, Mandal, and Calladine are only analogies, since they are solutions of different problems.

[3] On a finite domain this consequence is indeed simple; on an infinite domain it appears that not only the third-order term but also the fourth-order term in the energy has to be taken into account, as remarked in section 3.

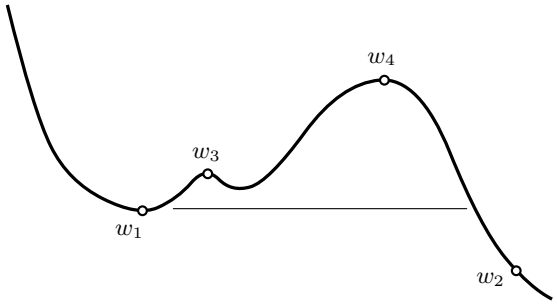

FIG. 6.1. *While a local algorithm for finding a critical point may settle on a minor critical point such as w_3, the mountain pass algorithm, by its global setup, will converge to the essential obstacle w_4.*

6.4. Scale-invariance of the localized solutions. It is an interesting observation that the von Kármán–Donnell equations can be rescaled to depend only on the (rescaled) load level. For localized solutions, for which the boundary plays no role of importance, this implies that the set of solutions reduces to a one-parameter family. This not only allows for efficient computation of the behavior of such solutions but also gives interesting insight into the relationship between dimples in cylinders of varying geometry (see, e.g., Figure 4.4).

Naturally the scale-invariance is expected to break upon replacing the von Kármán–Donnell equations with a different (probably more detailed) shell model. Nonetheless, it may be reasonably expected that much of the understanding of the relationship between cylinders of different geometries remains roughly correct.

We certainly also expect that the large-scale geometry of the energy landscape does not depend on the specific model of the cylinder. Using a discrete mountain pass algorithm to find mountain pass points therefore does not depend on the von Kármán–Donnell equations and should give similar results regardless of which shell model is used.

6.5. Connection with sensitivity to imperfections and "perturbation energy." Kröplin, Dinkler, and Hillmann [23]; Duddeck et al. [11]; and Wagenhuber and Duddeck [32] were the first to suggest an estimate of the stability of the unbuckled state in terms of the ratio of a "perturbation energy" (*Störenergie*) to the prebuckling energy. In early papers [23, 11] the perturbations are still fixed rather than determined, but from both the introduction and the final results in [32] it may be deduced that an optimization is done over all perturbations (although this is simultaneously contradicted on page 333 of [32]). Unfortunately, these papers do not provide enough details for determining exactly what the authors calculate.

There is one aspect in which our method can clearly be seen to differ from these earlier approaches. The discrete mountain pass algorithm takes into account *global* features of the energy landscape and provides a global measure of the separation barrier between two states that lie far apart. This is different from the papers mentioned above, in which the method uses only local information (reflected, for instance, in the assumption that the equilibria in question lie on the same bifurcation branch). This difference is illustrated in Figure 6.1, where a local analysis might find stationary point w_2, but the mountain pass algorithm will find the more important obstacle w_4.

Appendix A. Proof of Lemma 3.3. Lemma 3.3 states that *there exists a*

sequence of functions w_δ, 1-periodic on $\mathbb{R}^2$, such that

$$\int_{[-1/2,1/2]^2} w_{\delta x}^2 \sim 1, \qquad \int_{[-1/2,1/2]^2} \Delta w_\delta^2 = O(\delta^{-1}), \tag{A.1}$$

$$\text{and} \qquad \int_{[-1/2,1/2]^2} \Delta \phi_\delta^2 = O(\delta^{2-\alpha}) \quad \text{as} \quad \delta \to 0$$

for any $\alpha > 0$. Here the function ϕ_δ solves (2.5) *with periodic boundary conditions. In addition, w_δ and ϕ_δ satisfy* (2.6) *on the boundary of $[-1/2, 1/2]^2$.*

The proof consists of three parts. In the first part we construct the functions w_δ; in the second part we study the symmetry properties and the support of the right-hand side of (2.5); and in the third part we show that this sequence has the asserted scaling.

A.1. Construction of w_δ. Let f_δ be given by

$$f_\varepsilon''(s) = \begin{cases} \dfrac{1}{4\delta}, & \operatorname{dist}(s,\mathbb{Z}) < \delta, \\ 0 & \text{otherwise,} \end{cases} \qquad \text{with} \qquad f_\delta(0) = f_\delta'(0) = 0.$$

Note that f is even and that $f(1) = 1/4$. Define

$$w_\delta(x,y) = f_\delta(y+x) + f_\delta(y-x) - \frac{1}{2} f_\delta(2x) - \frac{1}{2} y^2.$$

We shall drop the subscript δ and simply write w and f.

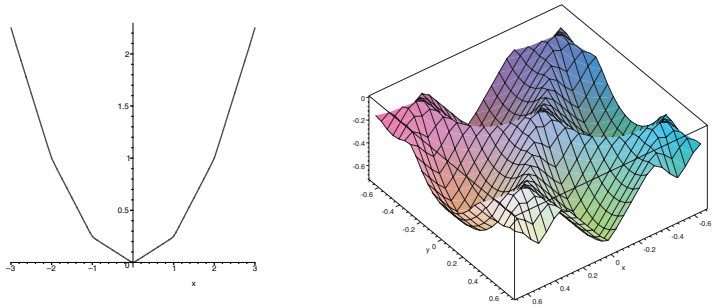

FIG. A.1. *The functions f and $-w$; on the right the plotting area is slightly larger than one period.*

The function w is periodic on $\mathbb{R}^2$ with period 1 in each direction. To show this, we prove that the first two derivatives match up on opposite sides of $[-1/2, 1/2] \times [-1/2, 1/2]$ as follows:

- By the symmetry of f, the function w is even in both x and y. Consequently w takes the same values on $(1/2, y)$ and $(-1/2, y)$; the same holds for $(x, \pm 1/2)$.
- For the comparison of the first derivatives, we calculate

$$\int_{-1/2}^{1/2} w_{xx}(x,y)\,dx = \int_{-1/2}^{1/2} f''(y+x)\,dx + \int_{-1/2}^{1/2} f''(y-x)\,dx - 2\int_{-1/2}^{1/2} f''(2x)\,dx = 0,$$

implying that $w_x(-1/2,y) = w_x(1/2,y)$; by the symmetry of w it follows that $w_x(-1/2,y) = w_x(1/2,y) = 0$. Similarly, using the definition of f_δ we find that

$$\int_{-1/2}^{1/2} w_{yy}(x,y)\,dy = \int_{-1/2}^{1/2} f''(y+x)\,dy + \int_{-1/2}^{1/2} f''(y-x)\,dy - 1 = 0,$$

implying that $w_y(x,-1/2) = w_y(x,1/2) = 0$.

Periodicity on $\mathbb{R}^2$ then follows from the remark that all second derivatives of w are periodic with period 1 in x and y.

A.2. Support, symmetry, and boundary conditions. Next we investigate the right-hand side of (2.5). We find

$$\begin{aligned}[w,w] + w_{xx} &= \big\{(f''(y+x) + f''(y-x) - 2f''(2x))(f''(y+x) + f''(y-x) - 1)\\ &\qquad - (f''(y+x) - f''(y-x))^2\big\}\\ &\qquad + (f''(y+x) + f''(y-x) - 2f''(2x))\\ &= 4f''(y+x)f''(y-x) - 2f''(2x)(f''(y+x) + f''(y-x)).\end{aligned}$$

This expression has a zero integral over $[-1/2,1/2]^2$. This follows from the periodicity of w,

$$\int_{-1/2}^{1/2}\int_{-1/2}^{1/2} w_{xx}w_{yy}\,dxdy = \int_{-1/2}^{1/2}\int_{-1/2}^{1/2} w_{xy}^2\,dxdy, \tag{A.2}$$

by partial integration. More is true, however; we analyze the support of $[w,w] + w_{xx}$ in $[-1/2,1/2]^2$ in more detail.

The value of f'' is either $(4\delta)^{-1}$ or zero; in order to determine $[w,w] + w_{xx}$ it is therefore sufficient to calculate the measures of the pairwise intersections of the supports of $f''(y+x)$, $f''(y-x)$, and $f''(2x)$ as follows:

- The intersection of the supports of $f''(y+x)$ and $f''(y-x)$ has total area $4\delta^2$ (see Figure A.2).
- The intersection of the supports of $f''(y+x)$ and $f''(2x)$ also has total area $4\delta^2$ (see Figure A.3).

Since the support of $[w,w] + w_{xx}$ is concentrated on a discrete set of points, let us examine the behavior at one of these points. For small δ the support forms disjoint sets in $[-1/2,1/2]^2$, and we can restrict our attention to the origin alone.

If $|s| < 1/2$, then $f_\delta''(s)$ can be written as

$$f_\delta''(s) = \frac{1}{\delta}\,g\left(\frac{s}{\delta}\right),$$

where

$$g(\sigma) = \begin{cases} \dfrac{1}{4}, & |\sigma| < 1,\\ 0 & \text{otherwise.}\end{cases}$$

Therefore, as long as $|(x,y)| < 1/4$, then

$$\begin{aligned}&4f_\delta''(y+x)f_\delta''(y-x) - 2f_\delta''(2x)(f_\delta''(y+x) + f_\delta''(y-x))\\ &\qquad = \frac{4}{\delta^2}\,g\left(\frac{y+x}{\delta}\right)g\left(\frac{y-x}{\delta}\right) - \frac{2}{\delta^2}g\left(\frac{2x}{\delta}\right)\left[g\left(\frac{y+x}{\delta}\right) + g\left(\frac{y-x}{\delta}\right)\right]\\ &\qquad = \frac{1}{\delta^2}\,F\big(\delta^{-1}(x,y)\big),\end{aligned} \tag{A.3}$$

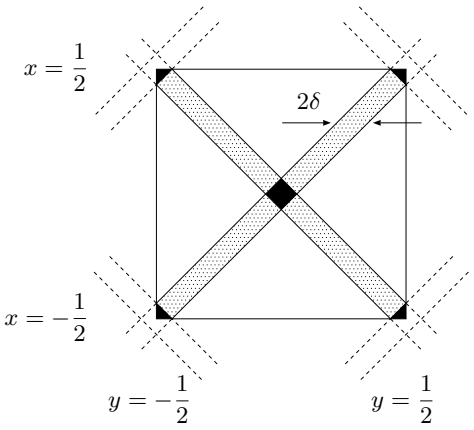

FIG. A.2. *The areas of the black regions add up to* $4\delta^2$.

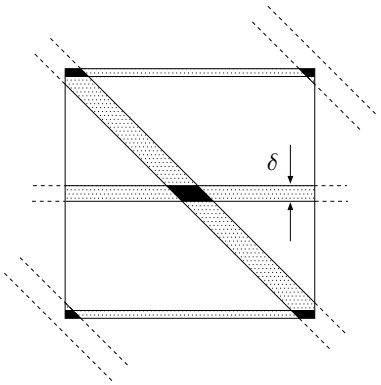

FIG. A.3. *The areas of the black regions add up to* $4\delta^2$.

where we introduce a new function F, which does not depend on δ, to summarize the line above. Note that $\operatorname{supp} F \subset [-2,2]^2$. Note also that by (A.2) the function F has zero integral; in addition, since f_δ'' is even, the function $4f_\delta''(y+x)f_\delta''(y-x) - 2f_\delta''(2x)(f_\delta''(y+x) + f_\delta''(y-x))$ is also even in x and in y. Therefore

$$\int_{\mathbb{R}^2} xF\big((x,y)\big)\,dxdy = \int_{\mathbb{R}^2} yF\big((x,y)\big)\,dxdy = 0.$$

This property will be used below.

The assertion also states that the functions w and ϕ satisfy (2.6) on the boundary of $[-1/2,1/2]^2$. We first note that w and ϕ are periodic in the following sense:

$$w(x \pm 1/2, y \pm 1/2) = w(x,y) \qquad \text{and} \qquad \phi(x \pm 1/2, y \pm 1/2) = \phi(x,y). \tag{A.4}$$

For w this is a simple consequence of the functional form of w; for ϕ it is a consequence of the uniqueness of solutions of (2.5) under periodic boundary conditions. The periodicity of w and ϕ in the y-direction in (2.6) then follows from a repeated application of (A.4). Similarly, the symmetry conditions in x in (2.6) follow from a combination of the symmetry of w and ϕ around $\{y = 0\}$ in combination with (A.4).

A.3. Scaling properties. We now use the information gathered above to show that the sequence w_δ has the scaling properties of (A.1). All function spaces are on $[-1/2,1/2]^2$.

First, f'_δ remains bounded on bounded sets as $\delta \to 0$; therefore $\int_\Omega w_{\delta x}^2$ converges to a finite, positive value. In addition, all second derivatives of w_δ remain bounded in L^1, so that

$$\|\Delta w_\delta\|_{L^1} \le C.$$

The second derivative f''_δ is bounded by $1/4\delta$, so that we can estimate

$$\|\Delta w_\delta\|_{L^2}^2 \le \|\Delta w_\delta\|_{L^1} \|\Delta w_\delta\|_{L^\infty} \le \frac{C}{\delta}.$$

Turning to ϕ_δ, we start by remarking that $[w_\delta, w_\delta] + w_{\delta xx}$ is bounded in L^1, since

$$\int_{|(x,y)|<1/4} \big|[w_\delta, w_\delta] + w_{\delta xx}\big| = \frac{1}{\delta^2} \int_{|(x,y)|<2\delta} \big|F\big(\delta^{-1}(x,y)\big)\big| = O(1).$$

Since $W^{2,p} \hookrightarrow L^\infty$ for all $p > 1$, the solution of

$$\Delta^2 \psi = h$$

satisfies

$$\|\Delta\psi\|_{L^{p'}} = \sup_\zeta \frac{\int_\Omega \Delta\psi\Delta\zeta}{\|\Delta\zeta\|_{L^p}} = \sup_\zeta \frac{\int_\Omega h\zeta}{\|\Delta\zeta\|_{L^p}} \le C\,\|h\|_{L^1} \frac{\|\zeta\|_{L^\infty}}{\|\zeta\|_{W^{2,p}}} \le C\,\|h\|_{L^1},$$

so that

$$\|\phi_\delta\|_{W^{2,p'}} \le C\,\|[w_\delta, w_\delta] + w_{\delta xx}\|_{L^1} \le C,$$

where $1/p + 1/p' = 1$. Using $W^{2,p'} \hookrightarrow C^{1,1-2/p'}$ we find

$$\|\phi_\delta\|_{C^{1,1-2/p'}} \le C\,\|\phi_\delta\|_{W^{2,p'}} \le C.$$

Writing, locally at the origin,

$$\phi_\delta(x,y) = \phi_\delta(0,0) + \nabla\phi_\delta(0,0)\cdot(x,y) + O\big(|(x,y)|^{2(1-1/p')}\big),$$

we find, by multiplying (2.5) by ϕ_δ and integrating,

$$\begin{aligned}
\|\Delta\phi_\delta\|^2_{L^2([-1/2,1/2]^2)} &= 2\int_{[-1/4,1/4]^2} \phi_\delta\big\{[w_\delta, w_\delta] + w_{\delta xx}\big\} \\
&= 2\frac{\phi_\delta(0,0)}{\delta^2} \int_{[-1/4,1/4]^2} F\big(\delta^{-1}(x,y)\big) \\
&\qquad + 2\frac{\nabla\phi_\delta(0,0)}{\delta^2} \cdot \int_{[-1/4,1/4]^2} (x,y) F\big(\delta^{-1}(x,y)\big) + O\big(\delta^{2(1-1/p')}\big) \\
&= O\big(\delta^{2(1-1/p')}\big),
\end{aligned}$$

since the zeroth and first moments of F are zero. Since p' may be chosen arbitrarily large, this estimate concludes the proof.

Appendix B. Derivation of the von Kármán–Donnell equations. The common aim of the many elastic shell theories is to approximate three-dimensional elasticity by a reduced description in which the unknowns are functions of not three but two spatial variables; see, for example, [6]. For the von Kármán–Donnell cylinder the central approximation is the *director Ansatz*, which states that a normal to the center surface remains normal through deformation. By this Ansatz the displacement is fully characterized by the displacement vector (u, v, w), a function of the two in-plane spatial variables x and y, where u, v, and w are the displacements in the axial (x-), tangential (y-), and radial directions, respectively. Apart from some rescaling, the function w is the same as the unknown w in the rest of this paper.

In the formulation of section 2 the unknowns u and v are replaced with the Airy stress function ϕ, which is derived by minimization with respect to the displacements u and v for fixed w. This minimization argument is well known in the context of the von Kármán plate theory and can be found in many textbooks. Determining the boundary conditions that the function ϕ satisfies, however, is not straightforward (see also the discussion in [27]), and it is for this reason that we now describe the argument in detail. The main goal is to show that the function ϕ is periodic in the tangential direction.

B.1. Energy and shortening. All quantities in this appendix are dimensional. We assume a cylinder of thickness t, length L, and radius R, and we set $\Omega = [0, L] \times [0, 2\pi R]$. The stored energy given by [31] is

$$E_1 = \frac{t^3 E}{24(1-\nu^2)} \int_\Omega \Delta w^2 + \frac{t}{2E} \int_\Omega \big[(\sigma_{11}+\sigma_{22})^2 - 2(1+\nu)(\sigma_{11}\sigma_{22} - \sigma_{12}^2)\big]$$

for a linear material of Young's modulus E and Poisson's ratio ν. Under the assumption of plane stress, the stress and strain tensors are related by

$$\sigma = \frac{E}{1-\nu^2}\big[(1-\nu)\varepsilon + \nu \operatorname{tr}\varepsilon\, I\big] = \frac{E}{1-\nu^2}\begin{pmatrix} \varepsilon_{11}+\nu\varepsilon_{22} & (1-\nu)\varepsilon_{12} \\ (1-\nu)\varepsilon_{12} & \varepsilon_{22}+\nu\varepsilon_{11} \end{pmatrix}, \tag{B.1}$$

and under the small-angle approximation the strain tensor can be expressed in the displacements as

$$\varepsilon = \begin{pmatrix} u_x + \frac{1}{2}w_x^2 & \frac{1}{2}u_y + \frac{1}{2}v_x + \frac{1}{2}w_x w_y \\ \frac{1}{2}u_y + \frac{1}{2}v_x + \frac{1}{2}w_x w_y & v_y + \frac{1}{2}w_y^2 - \rho w \end{pmatrix}. \tag{B.2}$$

These choices for the energy and for the stress and strain tensors are very similar to those for a flat plate. The intrinsic curvature of the cylinder, of magnitude $\rho = 1/R$, appears only in the last term of ε_{22}, $-\rho w$, which expresses the fact that radial displacement creates extensional strain in the y-direction.

The average axial shortening is given by

$$S_1 = -\frac{1}{2\pi R}\int_0^{2\pi R} \big[u(L,y) - u(0,y)\big]\, dy = -\frac{1}{2\pi R}\int_\Omega u_x \, dxdy,$$

and an equilibrium (u, v, w) at load level P is a stationary point of the total potential $V_1 = E_1 - PS_1$.

B.2. Boundary conditions. At the boundaries $y = 0, 2\pi R$ it is natural to assume that u, v, and w are periodic, but at $x = 0, L$ there is a certain amount of choice.

The boundary conditions on w (see (2.6a)) are

$$w_x = (\Delta w)_x = 0 \qquad \text{at } x = 0, L, \tag{B.3}$$

and these conditions signify a fixed angle ($w_x = 0$) and zero radial force ($(\Delta w)_x = 0$). They may also be understood as symmetry boundary conditions, as in the case of a sequence of cylinders stacked on top of each other. For u and v we assume boundary conditions

$$u_y = 0 \qquad \text{and} \qquad \sigma_{12} = 0 \qquad \text{at } x = 0, L, \tag{B.4}$$

which signify that the ends of the cylinder are rigid in the x-direction and that there is no friction between the cylinder and the apparatus holding it. Note that the pair of boundary conditions $\sigma_{12} = 0$ and $(\Delta w)_x = 0$ together states that the loading apparatus exerts only axial forces on the cylinder.

The boundary conditions on w are invariant under the addition of a constant to w, i.e., under the replacement of w with $w + c$; for stationary points we may exploit this fact.

LEMMA B.1. *If (u, v, w) is a stationary point of $E_1 - PS_1$ under boundary conditions* (B.3)–(B.4)*, then*

$$\int_\Omega \sigma_{22} = 0. \tag{B.5}$$

Proof. Under the replacement $w \mapsto w + c$, we have

$$\frac{d\sigma}{dc} = -\frac{E\rho}{1-\nu^2}\begin{pmatrix} \nu & 0 \\ 0 & 1 \end{pmatrix},$$

and therefore

$$\begin{aligned} 0 &= \frac{d}{dc}(E_1 - PS_1) \\ &= -\frac{t\rho}{1-\nu^2}\int_\Omega \big[(\sigma_{11} + \sigma_{22})(\nu + 1) - (1 + \nu)(\sigma_{11} + \nu\sigma_{22})\big] = -t\rho \int_\Omega \sigma_{22}. \end{aligned}$$

∎

B.3. Derivation of the Airy stress function ϕ. The energy (2.7) and the Airy stress function ϕ are derived from the total potential $E_1 - PS_1$ by minimization with respect to the displacements u and v for fixed w. Performing this minimization on the second term in E_1 yields the classical plate equilibrium equations

$$\sigma_{11x} + \sigma_{12y} = 0 \qquad \text{and} \qquad \sigma_{12x} + \sigma_{22y} = 0.$$

Note that the derivative of S_1 with respect to u only creates boundary terms. By applying three times the well-known characterization of divergence-free vector fields as rotations of scalar fields (see, e.g., [3, Thm. XII.3.5]) we obtain the *local* existence of a function ϕ satisfying

$$\sigma_{11} = E\phi_{yy}, \qquad \sigma_{12} = -E\phi_{xy}, \qquad \text{and} \qquad \sigma_{22} = E\phi_{xx}, \tag{B.6}$$

where we use the traditional scaling of ϕ by Young's modulus.

B.4. Boundary conditions on ϕ. The existence of the function ϕ is the result of a local differential-geometric argument, and as such gives no reason for ϕ to be periodic in y. The following theorem shows that after a normalization transformation, the function ϕ can indeed be assumed to be periodic in y, and may be taken to satisfy the same boundary conditions as the function w.

THEOREM B.2. *If u, v, and w are periodic in y and satisfy boundary conditions* (B.3)–(B.4)*, then there exists a function ϕ that satisfies*

$$\sigma_{11} - \frac{1}{|\Omega|}\int_\Omega \sigma_{11} = E\phi_{yy}, \qquad \sigma_{12} = -E\phi_{xy}, \qquad \text{and} \qquad \sigma_{22} = E\phi_{xx}; \tag{B.7}$$

is periodic in y; and satisfies boundary conditions

$$\phi_x = (\Delta\phi)_x = 0 \qquad \text{at } x = 0, L. \tag{B.8}$$

Remark B.3. Mechanically the normalization of ϕ with $\int_\Omega \sigma_{11}$ means that ϕ represents the *deviation* from the unbuckled in-plane stress state.

Proof. As discussed above, there exists a function ϕ satisfying (B.6); we will construct in stages a new function $\hat{\phi}$ which satisfies (B.7) and the boundary conditions.

We first convert condition (B.6) into (B.7). Set

$$p(x) := \frac{1}{2\pi R}\int_0^{2\pi R} \phi_{yy}(x,y)\,dy = \frac{1}{2\pi R}\big[\phi_y(x,2\pi R) - \phi_y(x,0)\big].$$

Since the second derivatives of ϕ can be expressed in terms of derivatives of u, v, and w, the second and higher derivatives of ϕ are automatically periodic in y. Therefore

$$\frac{d}{dx}p(x) = \frac{1}{2\pi R}\big[\phi_{xy}(x,2\pi R) - \phi_{xy}(x,0)\big] = 0,$$

implying that p is actually independent of x. (A mechanical argument provides the same result: $Etp(x) = t\int_0^{2\pi R}\sigma_{11}(x,y)dy$ is the total force applied at a virtual cut at level x, and mechanical equilibrium implies that this force is independent of x.) Therefore

$$|\Omega|\,p = 2\pi R\int_0^L p\,dx = \int_\Omega \phi_{yy} = \frac{1}{E}\int_\Omega \sigma_{11},$$

so that the new function

$$\tilde{\phi}(x,y) := \phi(x,y) - \frac{p}{2}y^2$$

satisfies (B.7). Note that this implies

$$\int_\Omega \tilde{\phi}_{yy} = 0. \tag{B.9}$$

We now turn to the periodicity in the y-direction. It remains to show that $\tilde{\phi}$, $\tilde{\phi}_x$, and $\tilde{\phi}_y$ are the same at $y = 0$ and $y = 2\pi R$. Again the periodicity of the second derivatives implies that

$$\frac{d^2}{dx^2}\big[\tilde{\phi}(x,2\pi R) - \tilde{\phi}(x,0)\big] = \tilde{\phi}_{xx}(x,2\pi R) - \tilde{\phi}_{xx}(x,0) = 0,$$

so that $\tilde{\phi}(x, 2\pi R) - \tilde{\phi}(x, 0) = ax + b$ for some $a, b \in \mathbb{R}$. Defining

$$\hat{\phi}(x, y) := \tilde{\phi}(x, y) - \frac{by}{2\pi R} = \phi(x, y) - \frac{p}{2}y^2 - \frac{by}{2\pi R},$$

the function $\hat{\phi}$ still satisfies (B.7), and

$$\hat{\phi}(x, 2\pi R) - \hat{\phi}(x, 0) = ax.$$

Finally, we find that

$$a = \hat{\phi}_x(0, 2\pi R) - \hat{\phi}_x(0, 0) = \int_0^{2\pi R} \hat{\phi}_{xy}(0, y)\, dy = \frac{1}{E}\int_0^{2\pi R} \sigma_{12}(0, y)\, dy \overset{(B.4)}{=} 0,$$

and therefore that $\hat{\phi}(x, 2\pi R) - \hat{\phi}(x, 0) = 0$ for all x. The same follows for $\hat{\phi}_x(x, 2\pi R) - \hat{\phi}_x(x, 0)$ by differentiation.

To show that ϕ_y also matches,

$$\frac{d}{dx}\big[\hat{\phi}_y(x, 2\pi R) - \hat{\phi}_y(x, 0)\big] = \big[\phi_{xy}(x, 2\pi R) - \phi_{xy}(x, 0)\big] = 0,$$

and therefore $\phi_y(x, 2\pi R) - \phi_y(x, 0)$ is constant in x; by (B.9) this constant is zero. This proves that $\hat{\phi}$ satisfies (B.7) and is periodic in y.

We finally discuss the boundary conditions at $x = 0, L$, and we follow the line of reasoning of [27]. By (B.4) and (B.1), $\varepsilon_{12} = 0$ at $x = 0, L$, so that by (B.3) and (B.4),

$$v_{xy} = \frac{\partial}{\partial y}(2\varepsilon_{12} - u_y - w_x w_y) = 0 \qquad \text{at } x = 0, L.$$

Therefore

$$\varepsilon_{22x} = v_{xy} + w_y w_{xy} - \rho w_x \overset{(B.4)}{=} 0 \qquad \text{at } x = 0, L.$$

Using $E\varepsilon_{22} = \sigma_{22} - \nu\sigma_{11}$, we then find

$$\hat{\phi}_{xxx} - \nu\hat{\phi}_{xyy} = \phi_{xxx} - \nu\phi_{xyy} = \frac{1}{E}\frac{d}{dx}(\sigma_{22} - \nu\sigma_{11}) = \varepsilon_{22x} = 0,$$

and by adding $(1 + \nu)\hat{\phi}_{xyy} = -(1/E)(1 + \nu)\sigma_{12y} = 0$ it follows that

$$(\Delta\hat{\phi})_x = \hat{\phi}_{xxx} + \hat{\phi}_{xyy} = 0 \qquad \text{at } x = 0, L,$$

which proves one part of (B.8).

From $\hat{\phi}_{xy} = -\sigma_{12}/E = 0$ we find that

$$\hat{\phi}_x(0, y) = c_0 \qquad \text{and} \qquad \hat{\phi}_x(L, y) = c_L \qquad \text{for all } y \in [0, 2\pi R].$$

Writing

$$2\pi R(c_L - c_0) = \int_\Omega \hat{\phi}_{xx} = \frac{1}{E}\int_\Omega \sigma_{22} \overset{(B.5)}{=} 0$$

we find that $c_L = c_0$. Now the function

$$\overline{\phi}(x, y) := \hat{\phi}(x, y) - c_0 x = \phi(x, y) - \frac{p}{2}y^2 - \frac{by}{2\pi R} - c_0 x$$

satisfies (B.7) and (B.8) and is periodic in y. This concludes the proof. ∎

Remark B.4. It is instructive to note that the periodicity of ϕ is a result of the specific choice of boundary conditions, and will in fact not hold if different boundary conditions are taken. For instance, if a tangential shear stress τ is applied at the cylinder ends (i.e., the cylinder is loaded under torsion), then the coefficient a in the derivation above will not vanish, and ϕ_x will not be periodic in y.

B.5. Putting it all together. By an elementary but lengthy calculation we find that ϕ, as provided by Theorem B.2, satisfies the equation

$$\Delta^2\phi + \rho w_{xx} + [w,w] = 0 \qquad \text{in } \Omega, \tag{B.10}$$

and that the second term in E_1 can be written as

$$\frac{tE}{2}\int_\Omega \Big[\Delta\phi^2 - 2(1+\nu)[\phi,\phi]\Big].$$

By the boundary conditions given by Theorem B.2 the second term vanishes, and the total stored energy functional can therefore be written as

$$E_2(w) := \frac{t^3E}{24(1-\nu^2)}\int_\Omega \Delta w^2 + \frac{tE}{2}\int_\Omega \Delta\phi^2.$$

Note that this energy is a function of w alone; the function ϕ in this definition is assumed to be given by (B.10), with the boundary conditions of Theorem B.2. Similarly, we rewrite the average shortening as

$$\begin{aligned} S_2(w) := S_1(u) &= -\frac{1}{2\pi R}\int_\Omega u_x \\ &\overset{(B.2)}{=} -\frac{1}{2\pi R}\int_\Omega \left[\varepsilon_{11} - \frac{1}{2}w_x^2\right] \\ &\overset{(B.1)}{=} -\frac{1}{2\pi RE}\int_\Omega \big[\sigma_{11} - \nu\sigma_{22}\big] + \frac{1}{4\pi R}\int_\Omega w_x^2 \\ &\overset{(B.7)}{=} -\frac{1}{2\pi R}\int_\Omega \big[\phi_{yy} - \nu\phi_{xx}\big] + \frac{1}{4\pi R}\int_\Omega w_x^2 \\ &= \frac{1}{4\pi R}\int_\Omega w_x^2. \end{aligned}$$

A stationary point w of $E_2 - PS_2$ satisfies the Euler equation

$$\frac{t^2}{12(1-\nu^2)}\Delta^2 w + \frac{P}{2\pi REt}w_{xx} - \rho\phi_{xx} - 2[w,\phi] = 0,$$

where again ϕ is related to w by (B.10). With the nondimensionalization

$$w = 4\pi^2 R\,\overline{w}, \qquad \phi = 16\pi^4R^2\,\overline{\phi}, \qquad x \mapsto 2\pi R\,x, \qquad y \mapsto 2\pi R\,y,$$

we then obtain (2.4) and (2.5), and the dimensional energy E_2 and average shortening S_2 above can be expressed in these variables as

$$E_2 = \frac{\pi^2t^3E}{6(1-\nu^2)}\int \Delta\overline{w}^2 + 32\pi^6tER^2\int \Delta\overline{\phi}^2, \qquad S_2 = 4\pi^3R\int \overline{w}_x^2. \tag{B.11}$$

REFERENCES

[1] B. O. Almroth, *Postbuckling behaviour of axially compressed circular cylinders*, AIAA J., 1 (1963), pp. 627–633.

[2] A. Ambrosetti and P. H. Rabinowitz, *Dual variational methods in critical point theory and applications*, J. Funct. Anal., 14 (1973), pp. 349–381.

[3] S. S. Antman, *Nonlinear Problems of Elasticity*, 2nd ed., Appl. Math. Sci. 107, Springer, New York, 2005.

[4] J. Arbocz and C. D. Babcock, *The effect of general imperfections on the buckling of cylindrical shells*, ASME J. Appl. Mech., 36 (1969), pp. 28–38.

[5] W. Ballerstedt and H. Wagner, *Versuche über die Festigkeit dünner unversteifter Zylinderunter Schub- und Längskräften*, Luftfahrtforschung, 13 (1936), pp. 309–312.

[6] Z. P. Bažant and L. Cedolin, *Stability of Structures: Elastic, Inelastic, Fracture and Damage Theories*, Oxford University Press, New York, 1991.

[7] F. J. Bridget, C. C. Jerome, and A. B. Vosseller, *Some new experiments on buckling of thin-wall construction*, Trans. ASME Aero. Eng., 56 (1934), pp. 569–578.

[8] Y. S. Choi and P. J. McKenna, *A mountain pass method for the numerical solution of semilinear elliptic problems*, Nonlinear Anal., 20 (1993), pp. 417–437.

[9] M. Deml and W. Wunderlich, *Direct evaluation of the worst imperfection shape in shell buckling*, Comput. Methods Appl. Mech. Engrg., 149 (1997), pp. 201–222.

[10] L. H. Donnell, *A new theory for buckling of thin cylinders under axial compression and bending*, Trans. ASME Aero. Eng., 56 (1934), pp. 795–806.

[11] H. Duddeck, B. Kröplin, D. Dinkler, J. Hillmann, and W. Wagenhuber, *Nonlinear computations in civil engineering structures*, in DFG Colloquium, Springer-Verlag, Berlin, 1989 (in German).

[12] M. Eßlinger, *Hochgeschwindigkeitsaufnahmen vom Beulvorgang dünnwandiger, axialbelasteter Zylinder*, Der Stahlbau, 39 (1970), pp. 73–76.

[13] P. R. Everall and G. W. Hunt, *Mode jumping in the buckling of struts and plates: A comparative study*, Int. J. Non-Linear Mech., 35 (2000), pp. 1067–1079.

[14] D. J. Gorman and R. M. Evan-Iwanowski, *An analytical and experimental investigation of the effects of large prebuckling deformations on the buckling of clamped thin-walled circular cylindrical shells subjected to axial loading and internal pressure*, Develop. in Theor. and Appl. Mech., 4 (1970), pp. 415–426.

[15] N. Hoff, W. A. Madsen, and J. Mayers, *Post-buckling equilibrium of axially compressed circular cylindrical shells*, AIAA J., 4 (1966), pp. 126–133.

[16] J. Horák, *Constrained mountain pass algorithm for the numerical solution of semilinear elliptic problems*, Numer. Math., 98 (2004), pp. 251–276.

[17] J. Horák, G. J. Lord, and M. A. Peletier, *Numerical Variational Methods Applied to Cylinder Buckling*, in preparation.

[18] J. Horák and P. J. McKenna, *Traveling waves in nonlinearly supported beams and plates*, in Nonlinear Equations: Methods, Models and Applications (Bergamo, 2001), Progr. Nonlinear Differential Equations Appl. 54, Birkhäuser, Basel, 2003, pp. 197–215.

[19] C. Hühne, R. Zimmerman, R. Rolfes, and B. Geier, *Sensitivities to geometrical and loading imperfections on buckling of composite cylindrical shells*, in Proceedings of the European Conference on Spacecraft Structures, Materials and Mechanical Testing, Toulouse, 2002.

[20] G. W. Hunt and E. Lucena Neto, *Localized buckling in long axially-loaded cylindrical shells*, J. Mech. Phys. Solids, 39 (1991), pp. 881–894.

[21] G. W. Hunt, M. A. Peletier, A. R. Champneys, P. D. Woods, M. A. Wadee, C. J. Budd, and G. J. Lord, *Cellular buckling in long structures*, Nonlinear Dynam., 21 (2000), pp. 3–29.

[22] W. T. Koiter, *On the Stability of Elastic Equilibrium*, Ph.D. thesis, Technische Hogeschool, Delft (Technological University of Delft), Holland, 1945; English translation issued as Tech. report NASA-TT-F-10833, NASA Center for Aerospace Information, Hanover, MD, 1967.

[23] B. Kröplin, D. Dinkler, and J. Hillmann, *An energy perturbation method applied to nonlinear structural analysis*, Comput. Methods Appl. Engrg., 52 (1985), pp. 885–897.

[24] G. J. Lord, A. R. Champneys, and G. W. Hunt, *Computation of localized post buckling in long axially-compressed cylindrical shells*, Philos. Trans. Roy. Soc. Lond. Ser. A, 355 (1997), pp. 2137–2150.

[25] G. J. Lord, A. R. Champneys, and G. W. Hunt, *Computation of homoclinic orbits in partial differential equations: An application to cylindrical shell buckling*, SIAM J. Sci. Comput., 21 (1999), pp. 591–619.

[26] M. A. Peletier, *Sequential buckling: A variational analysis*, SIAM J. Math. Anal., 32 (2001), pp. 1142–1168.

[27] D. Schaeffer and M. Golubitsky, *Boundary conditions and mode jumping in the buckling of a rectangular plate*, Commun. Math. Phys., 69 (1979), pp. 209–236.
[28] D. Smets and G. J. B. van den Berg, *Homoclinic solutions for Swift-Hohenberg and suspension bridge type equations*, J. Differential Equations, 184 (2002), pp. 78–96.
[29] M. Struwe, *Variational Methods*, Springer-Verlag, Berlin, 1990.
[30] R. C. Tennyson, *An Experimental Investigation of the Buckling of Circular Cylindrical Shells in Axial Compression Using the Photoelastic Technique*, Tech. Report 102, University of Toronto, Toronto, ON, Canada, 1964.
[31] T. von Kármán and H. S. Tsien, *The buckling of thin cylindrical shells under axial compression*, J. Aeronautical Sci., 8 (1941), pp. 303–312.
[32] W. Wagenhuber and H. Duddeck, *Numerischer Stabilitätsnachweis dünner Schalen mit dem Konzept der Störenergie*, Arch. Appl. Mech., 61 (1991), pp. 327–343.
[33] V. I. Weingarten, E. J. Morgan, and P. Seide, *Elastic stability of thin-walled cylindrical and conical shells under axial compression*, AIAA J., 3 (1965), pp. 500–505.
[34] T. A. Winterstetter and H. Schmidt, *Stability of circular cylindrical steel shells under combined loading*, Thin-Walled Structures, 40 (2002), pp. 893–909.
[35] W. Wunderlich and U. Albertin, *Analysis and load carrying behaviour of imperfection sensitive shells*, Int. J. Numer. Methods Engrg., 47 (2000), pp. 255–273.
[36] N. Yamaki, *Elastic Stability of Circular Cylindrical Shells*, Appl. Math. Mech. 27, North–Holland, Amsterdam, 1984.
[37] Y. Yoshimura, *On the Mechanism of Buckling of a Circular Shell under Axial Compression*, Tech. Report 1390, NACA, Washington, DC, 1955.
[38] E. Zhu, P. Mandal, and C. R. Calladine, *Buckling of thin cylindrical shells: An attempt to resolve a paradox*, Int. J. Mech. Sci., 44 (2002), pp. 1583–1601.